HEAVE DYNAMICS OF A SURFACE EFFECT SHIP

William Alonzo Dewey

HEAVE DYNAMICS OF A SURFACE EFFECT SHIP

by

WILLIAM ALONZO DEWEY

B. S., University of Utah
(1968)

SUBMITTED IN PARTIAL FULFILLMENT
OF THE REQUIREMENTS FOR THE
ENGINEERS DEGREE IN OCEAN ENGINEERING
AND MASTER OF SCIENCE IN MECHANICAL ENGINEERING
at the
MASSACHUSETTS INSTITUTE OF TECHNOLOGY

June, 1974

Thesis

HEAVE DYNAMICS OF A SURFACE EFFECT SHIP

by

William Alonzo Dewey

Submitted to the Department of Ocean Engineering and Department of Mechanical Engineering on May 10, 1974, in partial fulfillment of the requirements for the Engineer Degree and Master of Science.

ABSTRACT

The dynamics of the sidewall-type surface effect ship (SES) for vertical plane heave motion in response to waves are established through theoretical model and experimental investigation. The theoretical models are digitally simulated and compared to an experimental tow tank model SES (length to beam ratio of 6.5) for verification. The examination of transient and frequency responses provides insight into the fundamental dynamic characteristics.

Thesis Supervisor: Henry M. Paynter, Sc. D.

Title: Professor of Mechanical Engineering

Thesis Advisor: Martin A. Abkowitz, Ph. D.

Title: Professor of Ocean Engineering

ACKNOWLEDGEMENTS

I wish to express my appreciation for the guidance and encouragement that Professor Paynter gave throughout the term of this thesis. His interest made the thesis a pleasurable effort. Also, I thank Professor Abkowitz for his advice and cooperation in allowing me to use the MIT tow tank facility. My thanks to the typist, Delphine Radcliffe. Finally, I wish to especially thank my lovely wife, Gail, for her hours of critical review and perseverance.

TABLE OF CONTENTS

TABLE OF CONTENTS (continued)

LIST OF FIGURES

LIST OF FIGURES (continued)

LIST OF TABLES

NOMENCLATURE

A_b	Waterplane area of cushion, $\ell \cdot b$.
A_e	Exit air flow area.
A_{eb}, A_{es}	Bow and stern exit air flow areas.
A_o	Entrance air flow area.
A_{sw}	Sidewall waterplane area, $\ell \cdot y_{sw}$.
a	Added mass.
B	Beam overall.
b	Cushion width.
b_c	Cushion damping coefficient.
b_w	Sidewall damping coefficient.
b_1	$b_c + b_w$
C_e, C_o	Quadratic orifice coefficients.
F_1	External applied force.
g	Gravity constant.
h	Exit gap height.
h_o	Equivalent cushion height at equilibrium.
h_1	Equilibrium gap height.
k	Polytropic constant.
$\hat{k}_1$	Sidewall stiffness coefficient.
$\hat{k}_2$	Equivalent cushion stiffness coefficient.
$\tilde{k}_1$	Equilibrium buoyancy force on immersed sidewall, $2\rho V_{sw}$.
L	Length of SES overall.
ℓ	Length of cushion.
$*M_c$	Air mass in cushion region.
$*\dot{M}_f$	Supply flow rate.

*All equilibrium conditions are indicated by a zero subscript.

NOMENCLATURE (continued)

$\dot{M}_{in}$	Air mass flow rate into cushion.
$\dot{M}_{out}$	Air mass flow rate out of cushion.
m	Mass of the craft.
p_a	Ambient air pressure, absolute.
$*p_c$	Cushion air pressure, absolute.
$*p_s$	Supply air pressure from fan, absolute.
t	Time.
u	Craft forward velocity.
$*V_c$	Cushion volume.
V_d	Duct volume.
V_{sw}	Volume of immersed sidewall at equilibrium.
ω	Wave frequency.
ω_e	Encounter frequency.
ω_n	Natural frequency.
x	Horizontal position along craft length.
y_{sw}	Sidewall thickness.
z	Wave height at any point.
z_1	Vertical height of craft.
z_c	Cushion height.
z_{ob}	Water height inside cushion at bow.
z_{os}	Water height inside cushion at stern.
z_t	Sidewall height.
z_w	Average wave height inside cushion.
ξ	Damping ratio.
η_o	Wave height.

*All equilibrium conditions are indicated by a zero subscript.

NOMENCLATURE (continued)

λ	Wave length.
ρ	Water density.
ρ_a	Air density.
ρ_c	Cushion air density.
ρ_s	Supply air density.

CHAPTER I

INTRODUCTION

1.1 Background

In the past few years substantial interest has developed in surface effect ships (SES), specialized waterborne air cushion vehicles which can provide high speed waterborne transportation. The SES configuration being studied is of the captured air bubble type. It employs the air cushion vehicle principles, utilizing a pressurized compartment of trapped air to support the majority of the craft's weight. A smaller fraction of the total support force comes from the hydrostatic, hydrodynamic and aerodynamic forces. The pressurized compartment of air (cushion) is contained by rigid sidewalls along the craft length and by seals both fore and aft. See Fig. 1.1.

In the ocean environment, the principal vertical plane motions of interest from the aspect of seakeeping and habitability are heave, surge, and pitch. So as to provide reasonable estimates of these motions, effort is directed towards the development of tools that will provide information on the expected behavior of the full-scale craft. The principal tools used here are experimental model tests and mathematical simulation via digital computer.

The dynamic simulations are helpful where known Froude scaling laws do not hold. Since this is true of the heave-pressure coupled motion for the SES, then the simulation model becomes a very useful tool for full-scale motion prediction. This does not preclude the use of experimental scale models but, rather, it means that once digital simulations accurately predict experimental model results, then this new tool can be easily adjusted for known parameter changes. Therefore, it

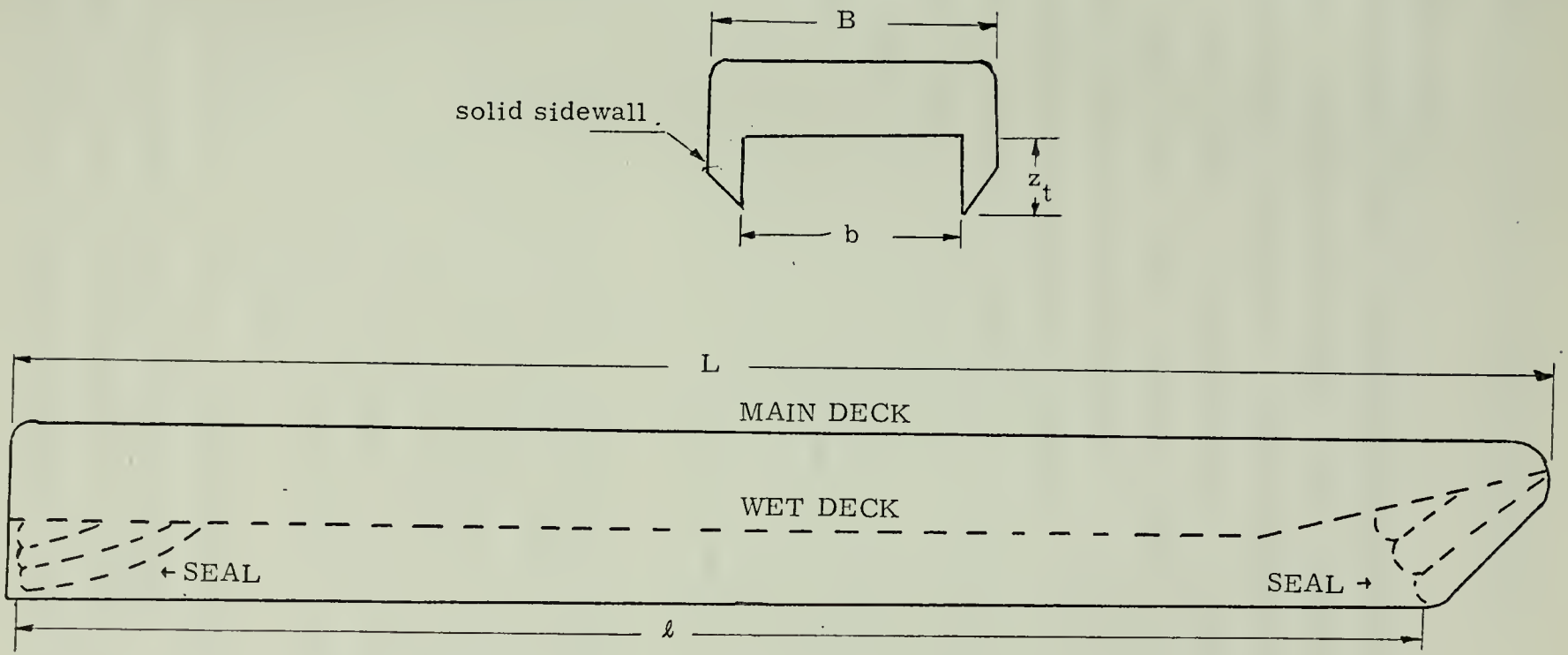

B = beam overall

b = beam of cushion

z_t = height of sidewall

L = length overall

ℓ = length of cushion

*See Appendix A for dimensions of Experimental SES Craft.

Fig. 1.1 SES Schematic.

can predict more accurately full-scale craft dynamics.

1.2 Scope of Thesis

The principal thrust of this thesis initially leads in two directions. These are (1) to develop a mathematical model of the equations of motion for digital simulation and (2) to build and test a scale model of an SES in the MIT tow tank facility. Attention is focused to the single degree of freedom in heave only. Heave motion of the SES, being the main contributor to the craft vertical acceleration levels, is a good starting point for digital simulation and experimental verification.

Chapter II explains the modeling of the fluid suspension system. The primary components to the model are developed for later use in the simulation Models A, B, and C found in Chapters III and IV where:

Model A is the SES craft transient performance analysis on cushion with no entrance or exit air flow. (Principally this is an inverted open-bottom container suspended by a pressurized air mass on the water surface.)

Model B is the same as Model A except, now, air flow is considered.

Model C is the simulated responses to regular waves.

The most basic model consists primarily of the following major components: (1) a cushion region formed under the craft that is maintained by low pressure air for craft support; (2) a nonflexible sidewall structure; (3) the forward and after seals; and (4) a fluid source for feeding air to the cushion.

The simulated transients and wave frequency analysis are to be compared to experimental model tests for verification. Comparisons of heave amplitude, phase and acceleration levels are illustrated, along with their time histories at selected frequencies. The experimental

model tests were conducted at zero forward speed.

1.3 Prior Work Related to Heave Motions

Historically there has been interest in the analysis of air suspension systems in heave from two major technologies: (a) the land-based air cushion vehicles, and (b) the sea-based air cushion craft. It is the latter field to which this thesis addresses itself, although useful information and analysis has been obtained from both areas.

The most recent and extensive analysis and simulation studies for SES craft have been conducted by Oceanics [1].* Simulation model analysis of the SES vertical plane dynamics has been performed, though verification is not extensive in the report.

Other land-based air cushion suspension studies have been conducted for the Department of Transportation at MIT [2 and 3], the results of which have been widely published.

---

*[ ] indicate references.

Note: From henceforward, "model" and "modeling" shall refer to the theoretical model for simulation. In order to avoid confusion in terminology, "experimental model" or "SES experimental craft" is used when referring to the tow tank test craft.

CHAPTER II

THE HEAVE SUSPENSION MODEL

2.1 The General Suspension Configuration

A nonlinear dynamic model for heave motion of a rigid body is developed for the configuration illustrated in Fig. 1.1. The basic suspension system consists of (1) cushion region, (2) supply system, (3) seal system, and (4) sidewalls. In the configuration a fan supplies flow through a constant volume duct and orifice restriction to the cushion chamber (plenum). The flow from the plenum escapes through the sealing gap area formed between the seal and the water surface. The fluid suspension is basically a three energy port device where energy transfer between the waves, air suspension and craft takes place as illustrated in Fig. 2.1. In developing models for these parts of the

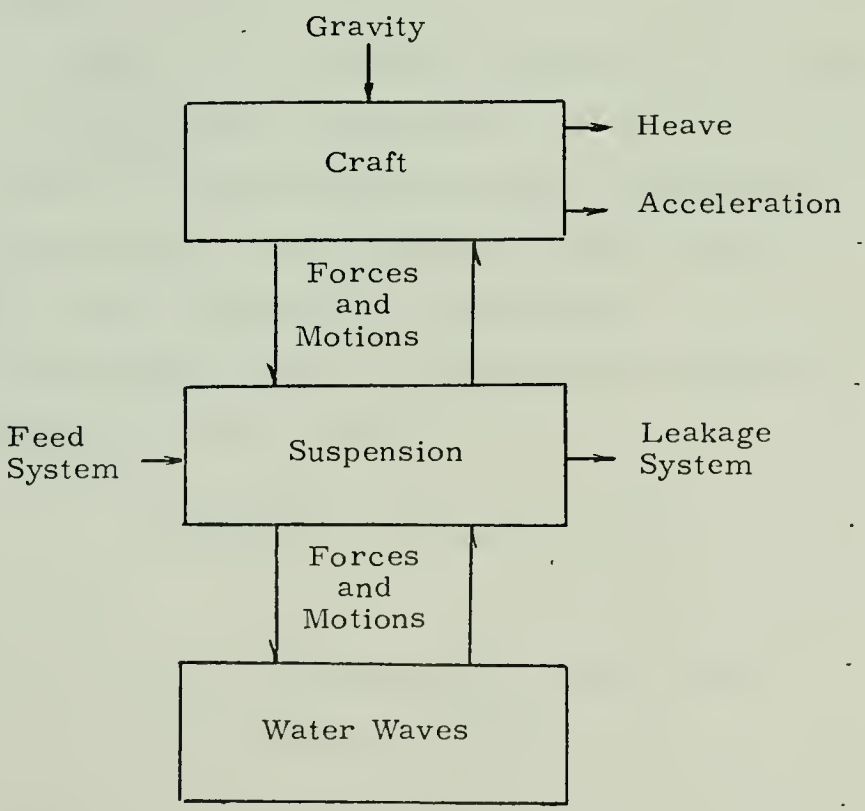

Fig. 2.1 Craft - Suspension - Wave System.

system, the following assumptions are made:

(1) The cushion and source absolute pressures are comparable to the absolute ambient pressure. For the experimental tow tank model the cushion pressure is on the order of one-tenth psig and the supply pressure of one to two psig.

(2) The external flow and pressure fields induced around the vehicle while it is moving with a forward velocity are not considered to affect the exit flow from the cushion. This assumption is not valid at high speeds, especially at the bow seal. Compensation for this effect could be modeled into the system for more extensive study.

(3) The cushion chamber base area A_b is constant.

(4) The pressure p_c and density ρ_c in the cushion region are spatially uniform.

(5) The Froude-Krylov hypothesis assumes the wave system is not appreciably altered by the presence of the craft. Thus, it is assumed that the wave is not diffracted or attenuated as it passes under the cushion chamber.

(6) The craft is assumed to be a rigid body.

The principal forces acting are identified in the rigid body equations of motion for heave, Fig. 2.2.

$$(m+a)\frac{d\dot{z}_1}{dt} = Z_c + Z_w + Z_s + Z_g \qquad (1)$$

where

$$\begin{aligned} Z_c &= \text{forces due to the cushion region} \\ &= -A_b (p_c - p_a) - b_c \dot{z}_1 \end{aligned} \qquad (1a)$$

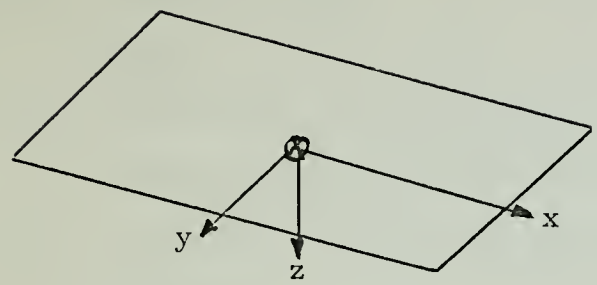

(a) Coordinate System.

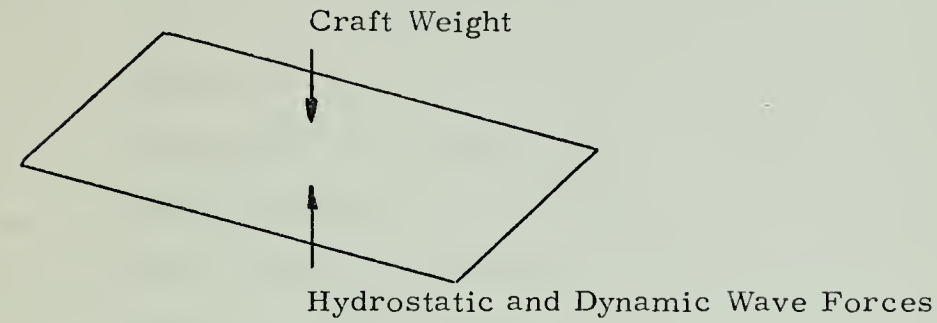

(b) Cushion Forces.

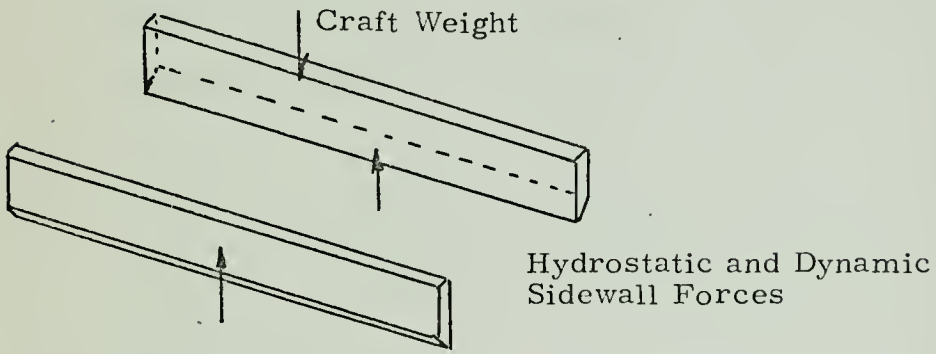

(c) Sidewall and Craft Forces

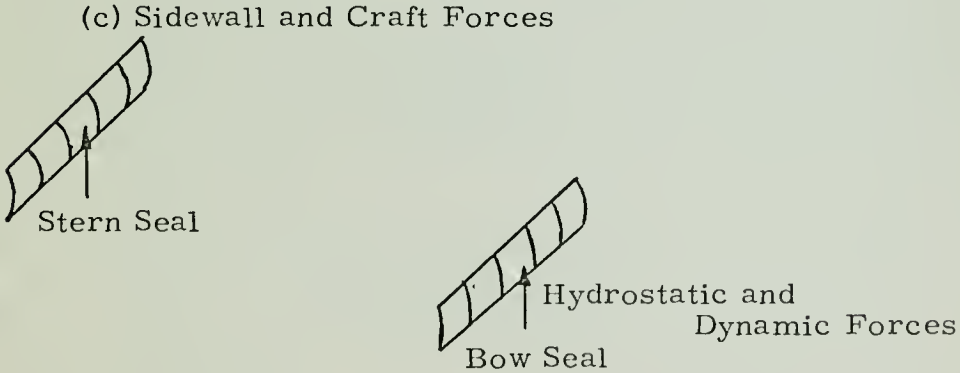

(d) Bow and Stern Seal Forces.

Fig. 2.2 Coordinates and Principal Heave Forces.

$$Z_w = \text{sidewall forces} \tag{1b}$$

$$= -\hat{k}_1(z_1 - z_w) - b_w \dot{z}_1 - \tilde{k}_1$$

$$Z_s = \text{forces due to seal (considered small compared to other external forces)} \tag{1c}$$

$$Z_g = \text{gravity and externally applied force} \tag{1d}$$

$$= mg + F_1$$

where

a = added mass

A_b = waterplane area of cushion base

A_{sw} = waterplane area of the sidewall

b_c = cushion damping coefficient

b_w = sidewall damping coefficient

F_1 = external force acting on the SES

$\hat{k}_1$ = stiffness coefficient of sidewall

$= 2\rho A_{sw}$

$\tilde{k}_1$ = vertical buoyant force of immersed sidewall $= 2\rho V_{sw}$

m = mass of craft

p_a = ambient pressure absolute

p_c = cushion pressure absolute

z_1 = craft position

z_w = average external water elevation

V_{sw} = volume of immersed sidewall at equilibrium

Therefore, substituting (1, a-d) into (1),*

$$(m+a)\frac{d\dot{z}_1}{dt} = -A_b(p_c-p_a) - b_1\dot{z}_1 - \hat{k}_1(z_1-z_w) - \tilde{k}_1 + mg + F_1 \qquad (2)$$

where

$$b_1 = b_c + b_w$$

In the analysis and later in the experiment, the forces acting on the seals were assumed to be relatively small compared to the cushion forces.

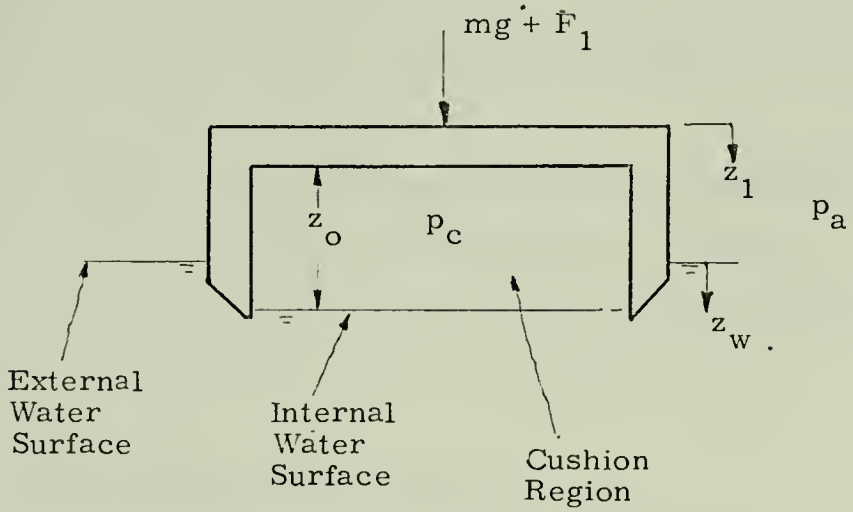

2.2 The Cushion Region Model

Within the plenum chamber, conservation of mass is required; thus, the inlet supply flow ($\dot{M}_{in}$) less the flow through the exit gap ($\dot{M}_{out}$) must equal the rate of change of mass within the chamber:

$$\frac{dM_c}{dt} = \dot{M}_{in} - \dot{M}_{out} \qquad (3)$$

M_c = air cushion mass

The pressure in the plenum chamber may be related to the mass (M_c) and chamber volume (V_c) by the equation of state. A polytropic relationship is assumed for the cushion chamber.

---

* ( ) indicate equations.

$$p_c = (M_c/V_c)^k \text{ constant} \tag{4}$$

The polytropic process is felt to be between isothermal (k = 1.0) and isentropic (k = 1.4).

The total cushion volume V_c at any instant in time may be expressed as the product of the base area A_b and the sum of the plenum equilibrium height h_o, craft elevation z_1, and the water surface elevation z_o.

$$V = A_b(-z_1 + h_o + z_o) \tag{5}$$

where

h_o = equivalent cushion height at equilibrium

z_w = average wave height under cushion

z_o = static depression of water plus the external wave elevation = $(p_c-p_a)/\rho + z_w$

2.3 Cushion Flow Entrance and Exit

From (3) the entrance flow $\dot{M}_{in}$ and exit flow $\dot{M}_{out}$ are modeled as follows. First, for purposes of the experimental craft verification the inlet mass flow $\dot{M}_{in}$ is considered constant since the entrance flow came from a high pressure source where the dynamics of the cushion region did not affect the mass flow to any degree. Secondly, in modeling an actual system where fan and duct dynamics are important, the mass flow into the cushion is modeled according to the classical quadratic orifice equation for non-compressible flow. Non-compressible flow may be assumed for the absolute source and cushion pressures since they are comparable to the absolute ambient pressure ($p_s-p_a = p_c-p_a \leq 1$ psi). Mass flow into the cushion is:

$$\dot{M}_{in} = C_o A_o (2(p_s - p_c)\rho_s/g)^{\frac{1}{2}} \quad (6)$$

The mass flow that exits from the plenum must either reverse and pass through the entrance orifice in the case where $p_c > p_s$ or the flow passes under the bow and aft seals. Again the $\dot{M}_{out}$ is modeled similarly to the entrance mass flow with the exception that now the exit leakage area A_e is varying.

$$\dot{M}_{out} = C_e A_e (2(p_c - p_a)\rho_s/g)^{\frac{1}{2}} \quad (7)$$

where

A_o = entrance flow area to cushion

A_e = variable exit flow area under seals

C_o, C_e = discharge coefficients (assume . 0.6)

p_s = fan supply pressure

2.4 Exit Air Flow Region

The exit area is the opening between the seal and the water surface through which the relatively low pressure air escapes at the bow and stern. This assumes that the sidewalls allow no leakage. The total leakage area is

$$A_e = A_{eb} + A_{es} \quad (8)$$

where

A_e = total exit area

A_{eb}, A_{es} = bow and stern leakage areas

The bow and stern exit areas are related geometrically to the craft

seals and water vertical position by:

$$A_{eb} = \begin{cases} b(-z_1 + z_{ob} + h_1) & \text{if } > 0 \\ 0 & \text{if } \leq 0 \end{cases} \tag{9}$$

$$A_{es} = \begin{cases} b(-z_1 + z_{os} + h_1) & \text{if } > 0 \\ 0 & \text{if } \leq 0 \end{cases} \tag{10}$$

where the wave height at the bow and stern respectively are given by:

z_{ob} = cushion water height at bow

z_{os} = cushion water height at stern

h_1 = equilibrium gap height

2.5 The Fluid Source and Feed System

This section on the fluid source is presented for future detailed studies where the duct and fan dynamics may influence the full-scale craft results. The fan and duct dynamics, as given here, were not needed for the verification of the experimental model tests. The use of a constant mass flow rate source in the experimental test apparatus made it feasible to focus attention directly to the fluid suspension (cushion) system. The feeding system which supplies air flow to the cushion in the full-scale craft consists of a fan and a feed duct. The fan may be, in general, assumed to operate at a constant supply pressure. This assumption is valid if the source pressure remains nearly equal to the fan operating point equilibrium pressure. However, for large deviations from the operating point, the change in supply pressure as a function of

supply flow should be considered.

The fan curves identified in Fig. 2.3 may be represented by the nonlinear functional relation:

$$\dot{M}_f = f(p_s - p_a) \tag{11}$$

Operation about the equilibrium point may be linearized for simulation and analysis wherein the mass flow rate $\dot{M}_f$ is given as:

$$\frac{\dot{M}_f}{\dot{M}_{fo}} = -\frac{1}{2}\left[\frac{p_s - p_a}{p_{so} - p_a}\right] + 2 \tag{12}$$

where

$\dot{M}_f$ = supply flow rate

$\dot{M}_{fo}$ = equilibrium supply flow rate

p_{so} = equilibrium supply pressure

The supply feeding duct is assumed to act as a fluid capacitance with duct resistance lumped into the plenum inlet supply area resistance.

The equation of state for a polytropic pressure density relationship similar to (4) combined with the conservation of mass may be written as:

$$\frac{V_d \rho_s}{k p_{so}} \dot{p}_s = \dot{M}_f - \dot{M}_{in} \tag{13}$$

where

ρ_s = supply air density

V_d = duct volume

2.6 External Disturbances

The transient performance study for Models A and B considers an instantaneous step increase in force F_1 applied to the model craft. In

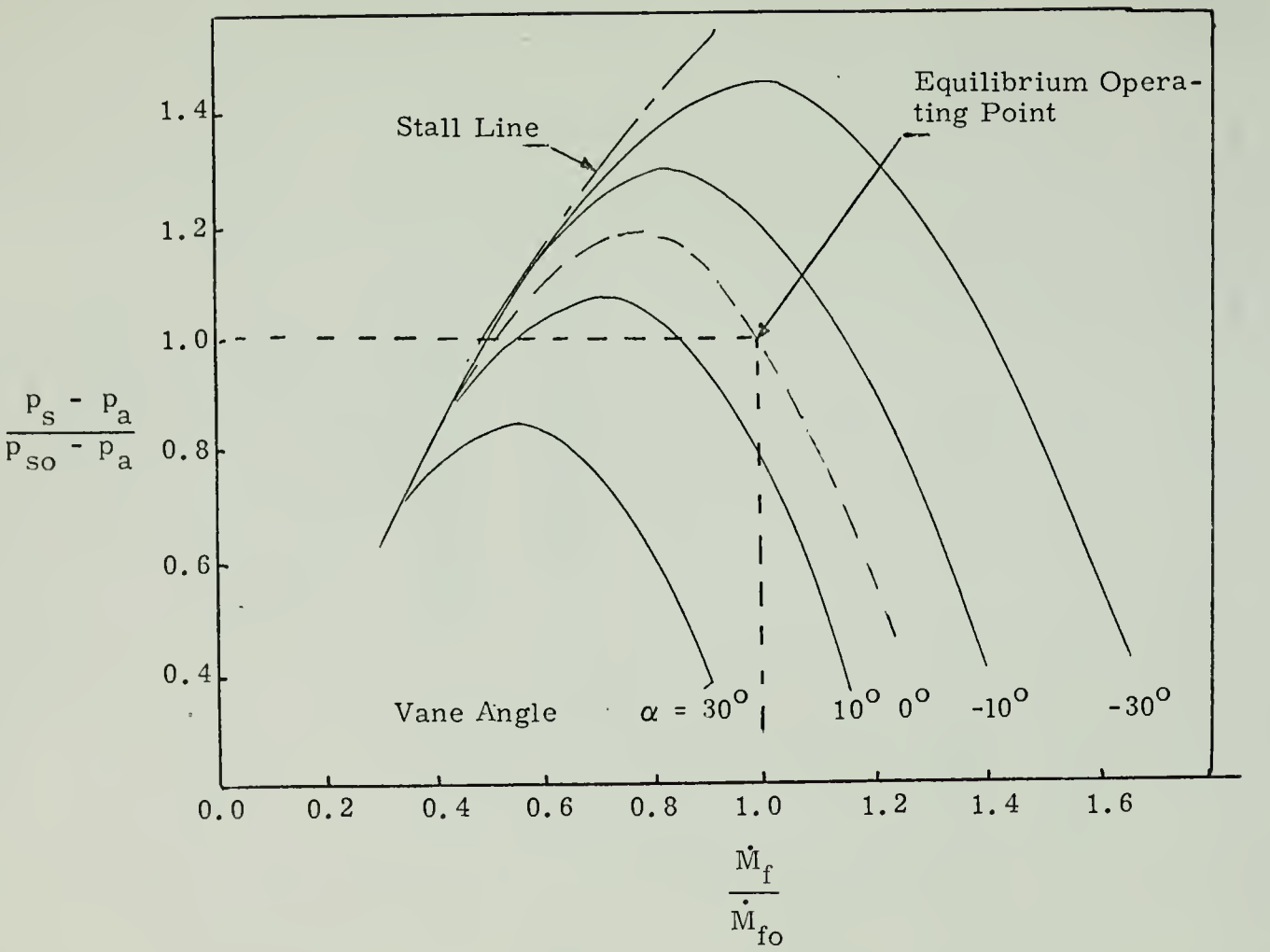

Fig. 2.3 Typical Compressor Characteristics.

the later study of Model C the external disturbance comes from the waves z_w. The external wave disturbance acts to change the air volume and hydrostatic force on the sidewalls.

The typical seaway considered in the analysis is a regular sinusoidal wave of height η_o and frequency ω. In the SES coordinate system, the origin is considered at the longitudinal center of gravity. Therefore the regular wave elevation for head seas is described by:

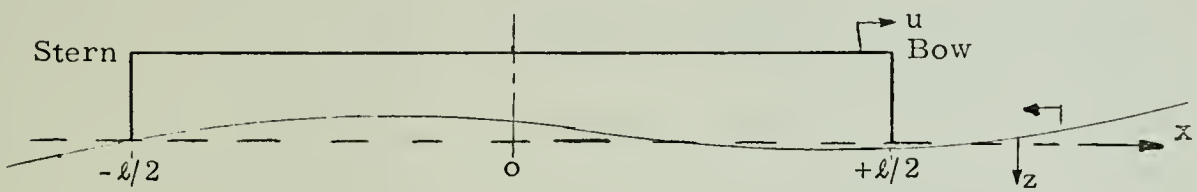

$$z = \eta_o \sin\left(\frac{2\pi x}{\lambda} + \omega_e t\right) \qquad (14)$$

where

ℓ = length between seals

η_o = wave height

λ = wavelength of wave

u = craft forward velocity

ω_e = encounter frequency = $\omega t + \omega^2 u/g$ for head seas

ω = wave frequency

x = position along craft length from midship positive forward

The instantaneous wave height along the length of the cushion and at the seals is important in the accurate model representation of the real system. In the first case the water height at the bow and stern seals acts as an external disturbance that changes the equilibrium gap height h_o caused by air flowing from the cushion under the seals. The wave height at the bow and stern seals, without taking into account the depression due to cushion pressure, is given by:

$$z_{ob} = \eta_o \sin(\omega_e t + \pi\ell/\lambda) \tag{15}$$

$$z_{os} = \eta_o \sin(\omega_e t - \pi\ell/\lambda) \tag{16}$$

The average wave height under the cushion is determined by integration along the cushion length. The average wave height under the cushion is given by:

$$z_w = \frac{\eta_o}{\ell} \int_{-\ell/2}^{\ell/2} \sin(2\pi x/\lambda + \omega_e t)\, dx$$

Therefore

$$z_w = \frac{\eta_o \lambda}{\ell \pi} \sin(\pi\ell/\lambda) \sin \omega_e t \tag{17}$$

This model is representative as long as the air pressure inside the cushion is considered a constant throughout and there is no localized wave pumping.

2.7 Combined Model Equations

The system equations defining the heave dynamics of the craft for Models A, B, and C in Chapters III and IV are given below. This includes the equations from sections 2.1 - 2.5.

(2) $dz_1/dt = \dot{z}_1$

$$(m+a)d\dot{z}_1/dt = -b_1\dot{z}_1 - \hat{k}_1(z_1 - z_w) - A_b(p_c - p_a) - \tilde{k}_1 + mg + F_1$$

$$(3)\quad dM_c/dt = \dot{M}_{in} - \dot{M}_{out}$$

$$(4)\quad p_c = (M_c/V_c)^k \text{ constant}$$

$$(5)\quad V_c = A_b(-z_1 + h_o + z_o)$$
$$\text{where } z_o = (p_c - p_a)/\rho + z_w$$

$$(6)\quad \dot{M}_{in} = C_o A_o (2(p_s - p_c)\rho_s/g)^{\frac{1}{2}}$$

$$(7)\quad \dot{M}_{out} = C_e A_e (2(p_c - p_a)\rho_c/g)^{\frac{1}{2}}$$

$$(8)\quad A_e = A_{eb} + A_{es} \qquad (18)$$

$$(9)\quad A_{eb} = \begin{cases} b(-z_1 + z_{ob} + h_1) & \text{if } >0 \\ 0 & \text{if } \leq 0 \end{cases}$$

$$(10)\quad A_{es} = \begin{cases} b(-z_1 + z_{os} + h_1) & \text{if } >0 \\ 0 & \text{if } \leq 0 \end{cases}$$

$$(11)\quad \dot{M}_f = f(p_s - p_c)$$

$$(13)\quad (V_d \rho_s / k p_{so})\, \dot{p}_s = \dot{M}_f - \dot{M}_{in}$$

2.8 Linearized Model Equations

A linearized set of equations for the heave mode was developed and used along with the nonlinear equations (18) for determining effects of cushion parameters. The linearized equations are given in state variable form for Models A, B, and C. Excluded from these three models are the duct and fan dynamics since the experimental SES was supplied from a constant mass flow source.

$$\frac{d}{dt}\begin{bmatrix}\Delta z_1\\ \Delta \dot{z}_1\\ \Delta M_c\end{bmatrix} = \begin{bmatrix}0 & 1 & 0\\ A_{21} & A_{22} & A_{23}\\ A_{31} & 0 & A_{33}\end{bmatrix}\begin{bmatrix}\Delta z_1\\ \Delta \dot{z}_1\\ \Delta M_c\end{bmatrix} + \begin{bmatrix}0 & 0\\ B_{21} & B_{22}\\ 0 & B_{32}\end{bmatrix}\begin{bmatrix}\Delta F_1\\ \Delta z_w\end{bmatrix} \tag{19}$$

$$\begin{bmatrix}\Delta p_c\end{bmatrix} = \begin{bmatrix}C_{11} & 0 & C_{13}\end{bmatrix}\begin{bmatrix}\Delta z_1\\ \Delta \dot{z}_1\\ \Delta M_c\end{bmatrix} + \begin{bmatrix}0 & D_{12}\end{bmatrix}\begin{bmatrix}\Delta F_1\\ \Delta z_w\end{bmatrix}$$

where

$$A_{21} = -(\hat{k}_1 + \hat{k}_2)/(m+a)$$
$$A_{22} = -b_1/(m+a)$$
$$A_{23} = -A_b C_{13}/(m+a)$$
$$A_{31} = -K_3 C_{11} - K_4(-1 + C_{11}/\rho)$$
$$A_{33} = -K_3 C_{13} - K_4 C_{13}/\rho$$
$$B_{21} = 1/(m+a)$$
$$B_{22} = (\hat{k}_1 - A_b D_{12})/(m+a)$$
$$B_{32} = -K_3 D_{12} - K_4(1 + D_{12}/\rho)$$
$$C_{11} = \partial p_c/\partial z_1 = \rho/(h_o \rho/kp_{co} + 1)$$
$$C_{13} = \partial p_c/\partial M_c = (h_o \rho/M_{co})/(h_o \rho/kp_{co} + 1)$$
$$D_{12} = \partial p_c/\partial z_w = -(\rho/(h_o \rho/kp_{co} + 1)$$

where

$$K_3 = C_o(2\rho_c/g)^{\frac{1}{2}} A_e/[2(p_{co} - p_a)^{\frac{1}{2}}]$$
$$K_4 = C_o(2\rho_c/g)^{\frac{1}{2}}\ 2b(p_c - p_a)^{\frac{1}{2}}$$
$$\hat{k}_2 = A_b C_{11}$$

CHAPTER 3

SURFACE EFFECT SHIP TRANSIENT RESPONSE

3.1 Introduction

The basic equations, as developed in Chapter 2 and summarized in 2.7 and 2.8, are considered in the study of the transient response to external inputs. The theoretical results of various responses are compared to experimental data for verification. Two theoretical models that closely repeat the experimental tests are designated by the titles, Model A (without air flow), and Model B (with air flow). As a result of the transient responses, the natural frequency and damping of the SES are obtained.

Prior to reading in detail the analysis in Chapters 3 and 4, turn to Appendix A for discussion of the experimental model and testing.

3.2 Transient Performance Parameters

In the transient performance analysis, linearized cushion model performance is compared to experimental test data. Response characteristics are determined for several types of disturbances which are explained in 2.6.

The Model A equations are representative of the heave dynamics of the SES on the air cushion without air flow passing through the boundaries of the craft. Basically, the Model A dynamic equations are second order wherein the craft vertical position z_1 and velocity $\dot{z}_1$ are the primary state variables. The cushion pressure and other desired outputs are dependent variables of this system. The results of this analysis are the determination of the craft natural frequency and damping. The experimental data transients are conducted while the craft remains

stationary in the horizontal plane.

From (18), Model A nonlinearized equations are given with the following conditions:

$$dM_c/dt,\ dM_f/dt,\ dp_s/dt,\ \dot{M}_{in},\ \dot{M}_{out} = 0$$

Upon linearization, the resultant equations in state variable form are listed in (19) where:

$$A_{23},\ A_{31},\ A_{33},\ B_{32},\ C_{13} = 0$$

The second order system's characteristic equation in linear form is:

$$(m+a)\ddot{z}_1 + b_1\dot{z}_1 + (\hat{k}_1 + A_b\rho/(h_o\rho/kp_{co} + 1))z_1 = 0 \qquad (20)$$

The quadratic equation indicates a natural frequency for the coupled heave-pressure mode given by:

$$\omega_n = \left[\frac{k_1 + A_b/(h_o/kp_{co} + 1)}{m + a}\right] \qquad (21)$$

The damping ratio (relative to the critical damping) is given by

$$\xi = b_1/(2\omega_n(m+a)) \qquad (22)$$

In (20) the numerator terms are a measure of the system's stiffness. The first term k_1 is the stiffness coefficient of the sidewalls. The second group of terms of the numerator is the stiffness coefficient due to the air cushion. It should be noted that the theoretical stiffness coefficient is approximately equal to the waterplane area of the cushion and sidewalls times the water density.

All parameters of the second order system can be determined directly (see Table A.1) except for the damping b_1 and added mass a.

Estimates of these two variables may be derived from comparison of the transient heave response of the model and experiment. As a check on these results from theory [5], estimates of the damping and added mass for oscillating pressure fields on a free surface, as formulated by Stoker (1957), were used. Curves for added mass and damping from [5] are found in Appendix B. Note that, in order for correlation between experiment and theory to be valid, the seal and sidewall effects must also be estimated since 19% of the total waterplane area is due to the sidewall.

Figure 3.1 is the response for a step input in force acting on the craft. This force was 37.5 lb, equal to 100% of the craft weight. The natural frequency and critical damping ratios, calculated by comparing the digital response and experimental data, are approximately:

$$\omega_n = 9.2 \text{ rad/sec}$$
$$\xi = 0.3$$

where m = 1.16, a = 4.34 (lb sec^2/ft), $k_1 + k_2$ = 461 lb/ft, b_1 = 30 lb sec/ft.

Determination of the added mass, a, from theory based upon a two-dimensional oscillating pressure field [5] was in agreement with the experimental results. Theory from [5] (see Appendix B), indicates that the damping ratio due to the cushion is on the order of $\xi = 0.3$. This appears to agree well enough with the experimental results, though some discrepancy due to the sidewalls is certain to be present. Reference [1] indicated, though, that the damping due to the pressure field is negligible, which is contrary to what [5] and experimental results indicated.

In this study it was expected that there would be more of a

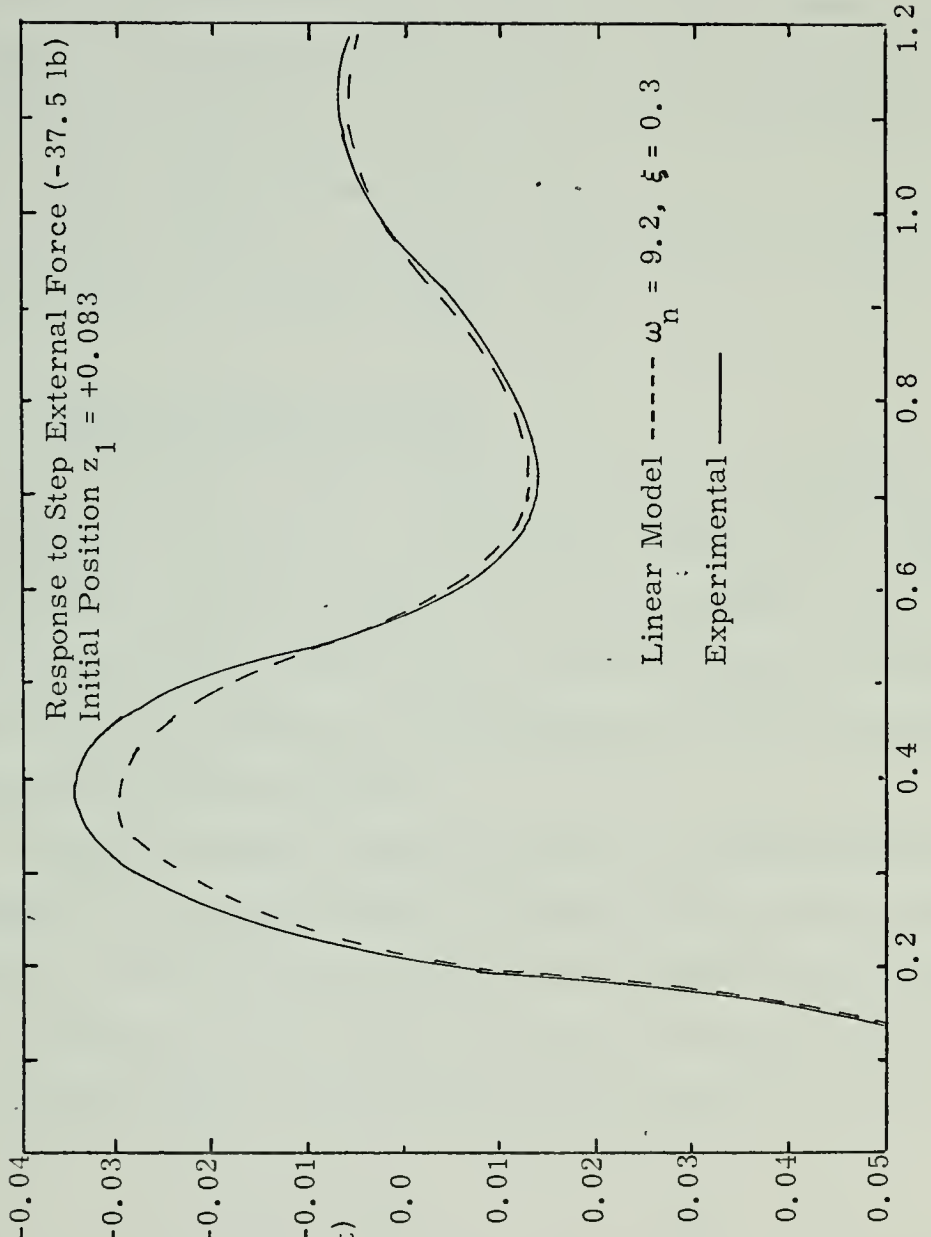

Fig. 3.1 Comparison of Model and Experimental Transient Response for Model A (No Air Flow).

difference between theory, based solely upon the cushion dynamics [5], and the experimental results. This is because the experimental craft had solid sidewalls and seals which covered 19% of the total waterplane area affected. But, within the accuracy of the experimental results, no detectable difference was found. Some theoretical estimates of the hydrodynamic force terms for the sidewalls could be found through the use of slender body theory, but for this thesis no such estimates are made. Future studies should look into this.

Typical velocity, acceleration and pressure transients corresponding to Model A are shown in Fig. 3.2.

3.3 Model B Transient Response

The transient response analysis for Model B is performed in the same manner as in Model A. The principal addition to the dynamic equations is the entrance and exit mass flows described in (3). The entrance mass flow is assumed to be a constant while the exit mass flow is described by the quadratic orifice equation (7) where the exit area and cushion pressure vary with time.

Again the resultant natural frequency ω_n and damping ratio ξ are determined. The state variables of the third order system are heave z_1, velocity $\dot{z}_1$, and air cushion mass M_c. The resultant output variables that are observed are the cushion pressure p_c and acceleration $\ddot{z}_1$. The model equations from (18) have the following conditions imposed:

$$dM_c/dt,\ dp_s/dt = 0 \quad \text{and} \quad \dot{M}_{in} = \text{const.}$$

Upon linearization, the resultant equations in state variable form are listed in (19). These equations are used in the transient response study.

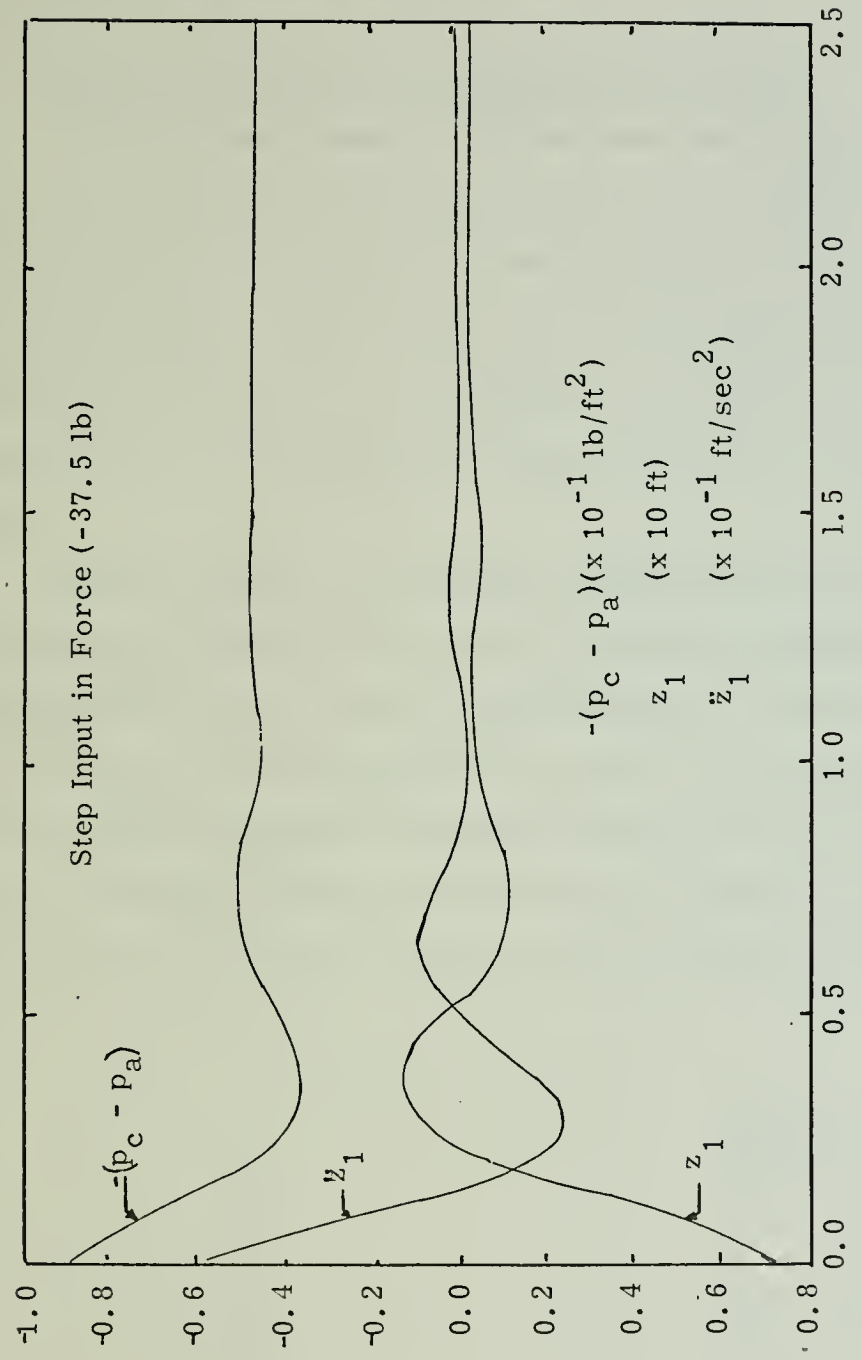

Fig. 3.2 Model A Transient Response Simulation.

Prior to comparing model simulations to test data, some observations of the experimental tests are made.

3.4 Transient Response from Experimental Tests

The SES experimental model response with air flow through the seals presented some interesting observations. Figure 3.3 shows two transient response curves for two test conditions nearly identical except for the seal design. Since the seals used in the experiments were non-flexible, the mass air flow rate would be expected to vary more dramatically here than for a design using a flexible seal that contours the water surface.

In test 1 of Fig. 3.3, the heave response shows a flattening at the top of the curve when the craft rises to 0.02' above equilibrium. In test 2 the craft rises to 0.038' above equilibrium. Why the difference?

In test 1 the seal design was such that a vertical gate seal of $\frac{1}{4}$" thick plexiglass was used to contain the cushion at the bow and aft. In this case the exit gap length was very short, resulting in a more rapid bleed-off of air. In test 2 the seal was much thicker (2 inches). This

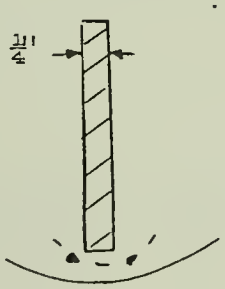

Seal design
for test 1.

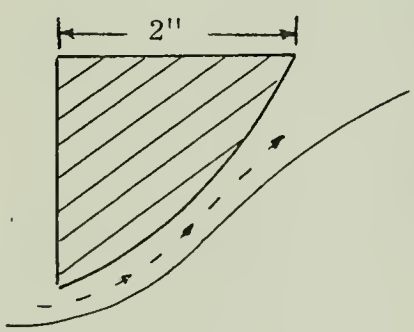

Seal design
for test 2.

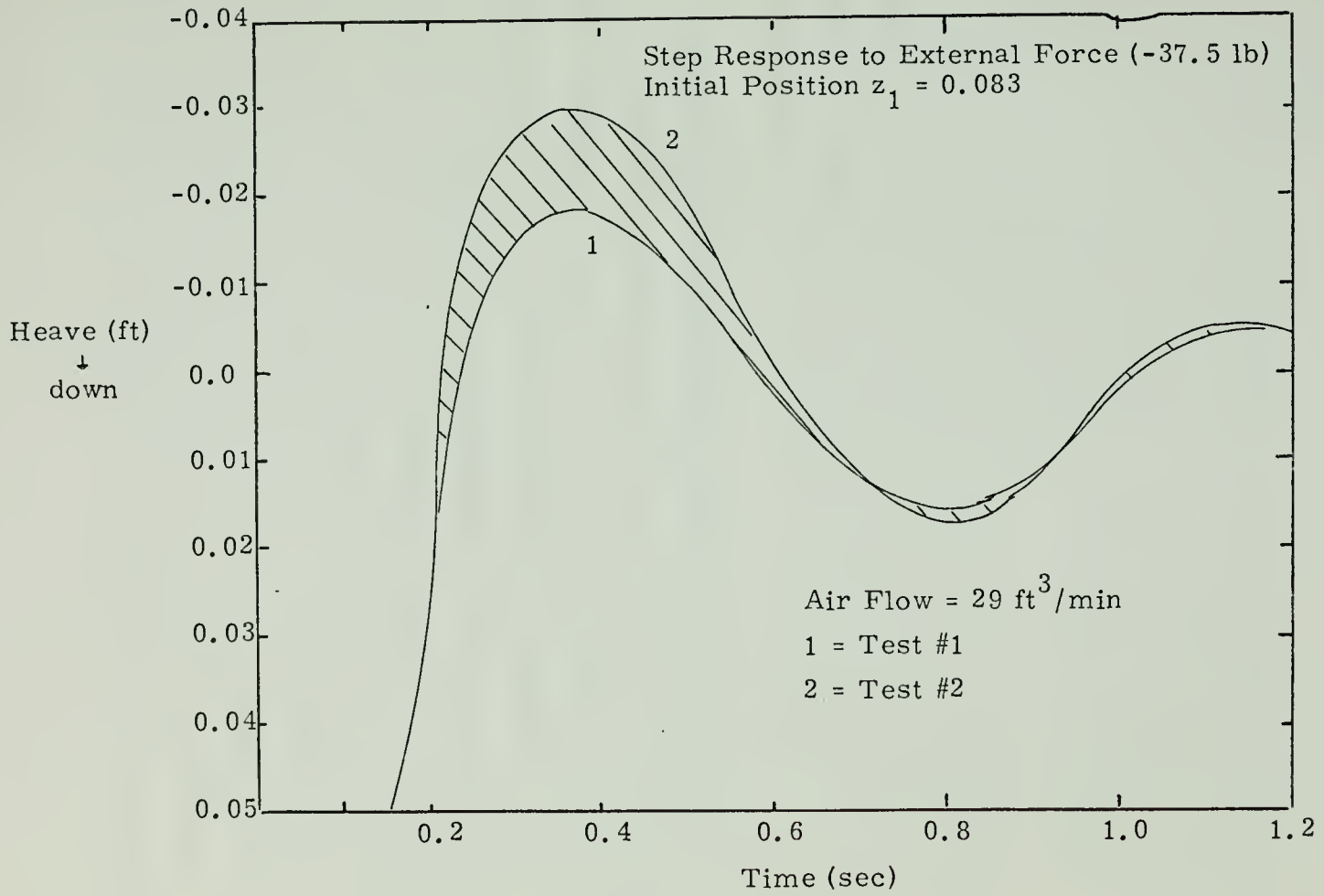

Fig. 3.3 Experimental Step Response of Model B (With Air Flow).

seal is faired to allow the water to flow smoothly around it without creating excess turbulence. The air escaping under the seal has to travel a larger distance before escaping from the plenum. For this reason the air loss is less, and the mean pressure level inside the cushion is higher.

As a result of the seal design, the heave response of test 2 has a higher overshoot than in test 1. The corresponding pressure drops in tests 1 and 2 were 8.6 and 7.2 lb/ft^2, respectively. Therefore, the seal design can be expected to influence the response. All further experimental tests use the thick seals.

Another important observation, which is not in the simulation, is the standing wave that is observed being created by the seals. This has the effect of causing local fluctuations in cushion volume and the exit air gap other than the normal rise and fall of the water level.

3.5 Comparison of Simulation and Experimental Transients

The transient response curve for the linearized equations is compared to the test data in Fig. 3.4. The natural frequency for the linearized equation of $\omega_n = 9.2$ rad/sec is the same as in Model A. The curves of lower damping are representative of the real situation where the faired seal (test 2) is used. This has a damping ratio on the order of $\xi = 0.3$. The experimental response (test 1) has a $\xi = 0.4$ for the first quarter cycle of the nonlinear response. The addition of nonlinearity in the exit gap area causes more overshoot, with the same value of $\xi = 0.3$, than was found in the totally linearized model equations. The value of $\xi = 0.3$ is carried through to the frequency response analysis.

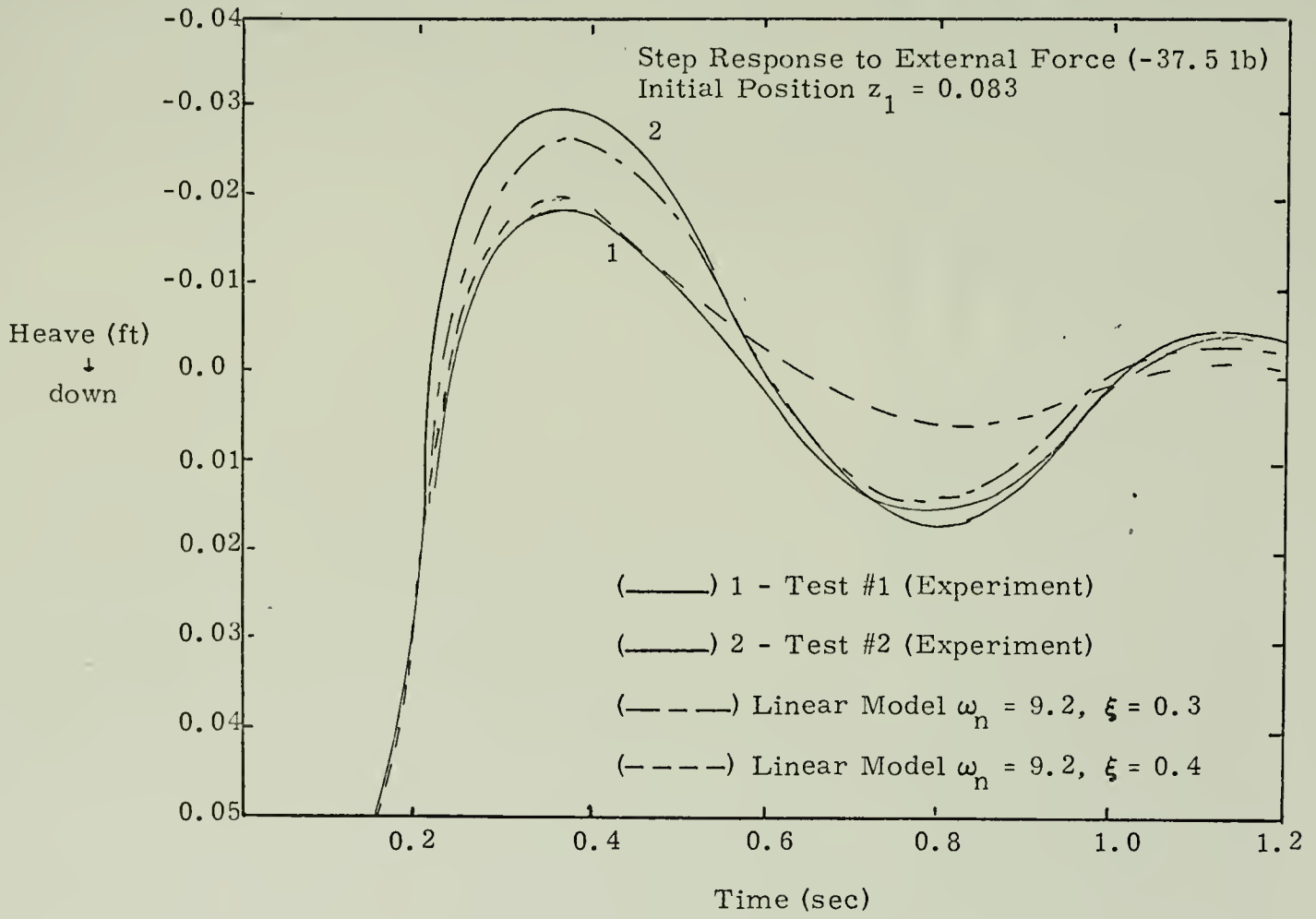

Fig. 3.4 Comparison of Linear Model B and Experimental Transients.

Another result of the Model B is that the addition of the air mass flow has little effect upon the natural frequency and critical damping when compared to Model A without air flow. This is a very likely result since the time constant for filling the air cushion region is long compared to the wave frequency.

The last comparison to be made is the acceleration and pressure responses, Fig. 3.5, of the digital simulation and experimental tests. Agreement appears to be quite good except for the higher frequency oscillations which are thought to come from the bubbling action of the air through the water around the seals. Also some impact forces may be caused by the water slapping the seals. These localized dynamic responses are not accounted for in the Model B.

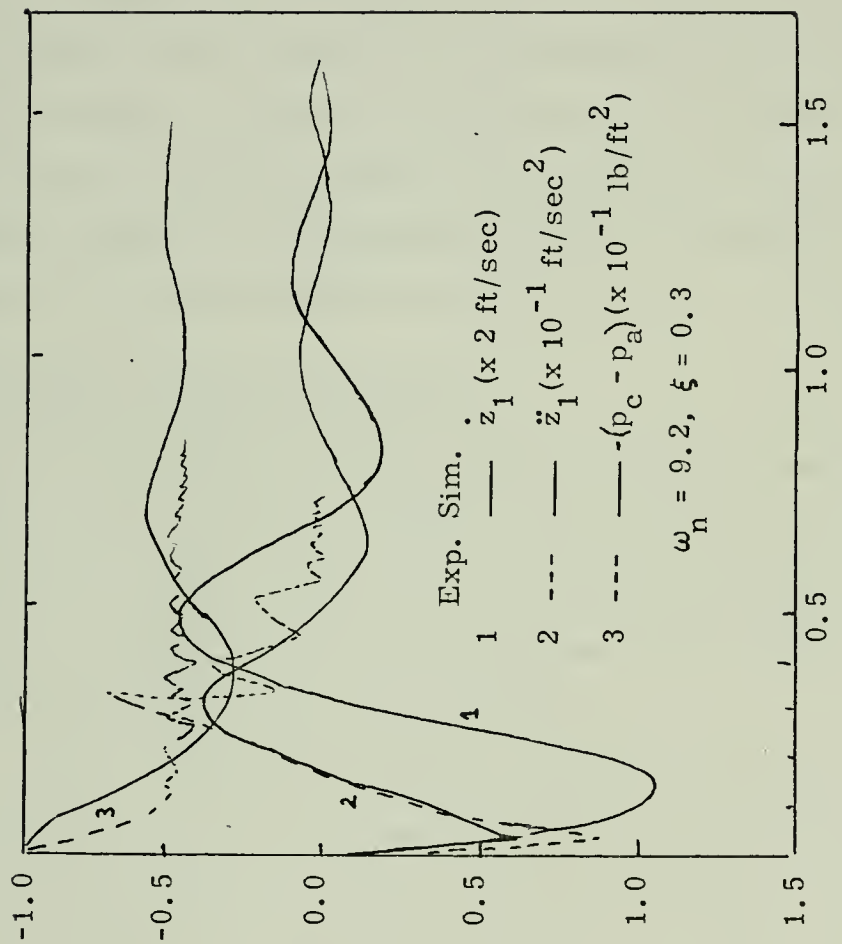

Fig. 3.5 Comparison of Step Response in Pressure and Acceleration.

CHAPTER 4

SES FREQUENCY RESPONSE TO REGULAR WAVES

4.1 Introduction

With the conclusions of the transient response the following chapter presents the frequency response analysis. Heave motion is the principal dynamic response to be analysed, since it can be easily compared to experimental data. Information on acceleration and cushion pressure is also presented. The behavior in regular waves was measured in the tow tank with the SES craft constrained to heave only and operating at zero forward velocity. The simulation model is presented first and then compared to the experimental results.

4.2 Model C Frequency Response

The modeling of the heave dynamic frequency response is primarily based on linear theory with certain nonlinear effects also included. The linearized equations of Model C, as developed in Chapter 2, are included in (19). The third order system equations are the same as given in Model B except for the following additions:

1. The external disturbances considered are the wave pumping (17) and the wave elevation at the bow and stern seals, (15) and (16).

2. The principal nonlinearity that is included in the systems equations is the gap exit area (9), (10) and (11), wherein the leakage area is allowed to vary as a function of the craft seal elevation and wave height. The model considers a nonflexible seal attached to the bow and stern. With the craft stationary in the x-y plane, air leakage exits from both seals. When the craft is moving forward then the principal leakage is from the stern seal only.

3. The body suspension forces acting on the craft, aside from the pressure force, represent the hydrostatic and hydrodynamic effects due to body-fluid interaction (including wave-induced effects) for the sidewalls. Estimates for added mass and damping come from the transient analysis and [5].

4.3 Heave Suspension Performance

In order to illustrate the nature of the craft responses to waves, digital computer simulations and experimental time histories are presented. The results of typical simulations appear in Fig. 4.1. The responses to regular waves illustrate the magnitude and phase of the heave, acceleration and pressure to the input. The constraint on the leakage area given by $A_b \geq 0$ is presented to illustrate the basic nature of the outputs. All motions are quite regular and the variation in gap area is the only nonlinearity. The behavior of the vertical CG acceleration is approximately proportional to but slightly lagging the pressure as the wavelength increases. The heave mean position, though not shown in Fig. 4.1, shifts downward as the gap area increases until a new equilibrium position is attained.

Figure 4.2 illustrates typical time histories of the motion found during the experiments in the tow tank. Several comparisons between the simulations, Fig. 4.1, and experiments, Fig. 4.2, are made:

1. Note the nonlinearity in the experimental heave response. The air leakage at the bow and stern appears to be causing the majority of the nonlinearity. The simulation model of the air gap leakage is more linear.
2. The experimental heave motion shows significant flattening of the response near the peak, which does not appear in the linear

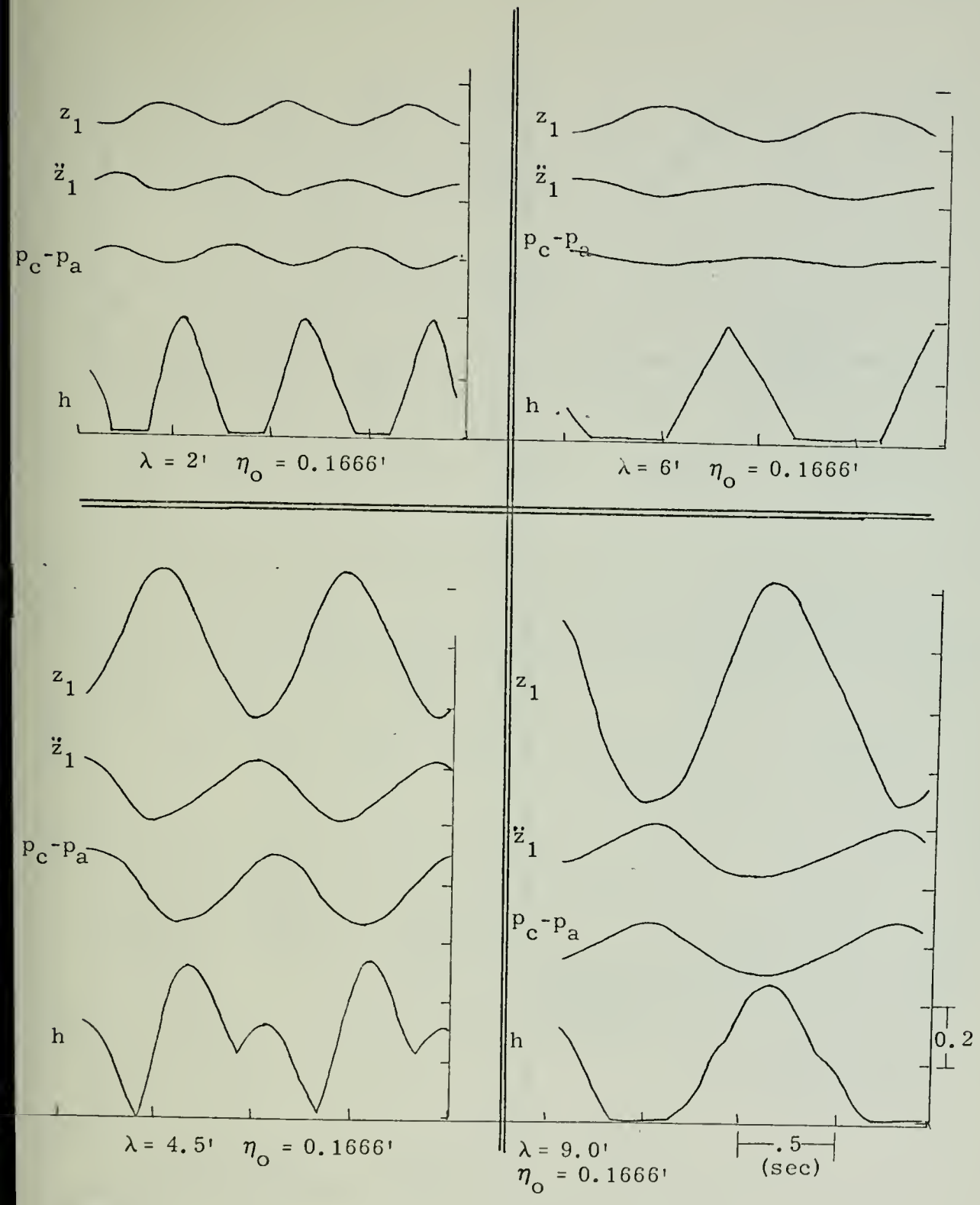

Scale: $z_1 \times 10$, ft $\quad (\rho_c - \rho_a) \times 10^{-1}$, lb/ft

$z_1 \times 10^{-1}$, ft/sec^2 $\quad$ h x 5, ft

Fig. 4.1 Simulated Heave Time Histories of SES to Regular Waves.

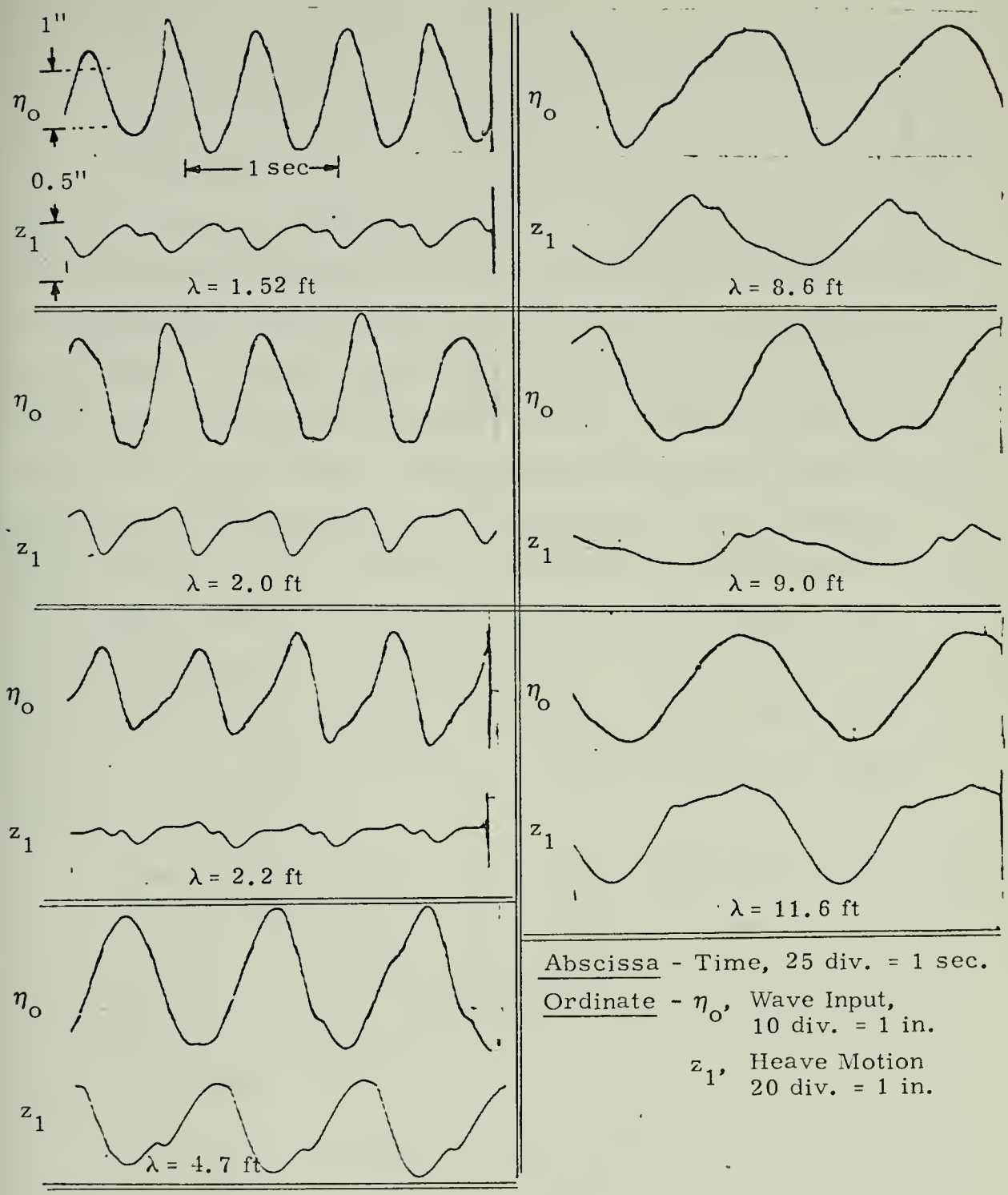

Abscissa - Time, 25 div. = 1 sec.

Ordinate - η_o, Wave Input, 10 div. = 1 in.

z_1, Heave Motion 20 div. = 1 in.

U = 0
Head Seas
Wave Height Ave. = 2 in.

Fig. 4.2 Experimental Heave Motion Time Histories for SES.

simulations.

3. The heave motion lags the wave input and is fairly consistent between experiment and simulation.

The pressure and acceleration time histories from several experimental results are presented in Fig. 4.3. The high frequency oscillations in the pressure and accelerations are felt to be caused by the air escaping under the seal due to the bubbling action which transmits pressure pulses. Likewise, they appear in the acceleration. The high frequency oscillations occur when the craft is reaching its peak in heave and the air exit gap opens. These high frequency oscillations, being due to local effects around the seals, should be given careful attention in future studies. The high frequency oscillations, though, appear to have little effect in the overall heave motion prediction when comparisons between simulation and experiment are made on the macro level. In addition, the solid seals attached to the craft are transmitting the forces due to the wave impact on the seals. A flexible seal should result in lower wave impact force.

In order to give a better picture of what is taking place overall, let us analyse the heave dynamics over a range of wavelengths. The heave motion (rms), Fig. 4.4, from the digital simulation indicates a behavior somewhat similar to that indicated by the limit value given in (23), with near zero response at values of

$$\lim |z_1| = \frac{\eta_o \lambda}{\ell \pi} \sin\left(\frac{\pi \ell}{\lambda}\right) \tag{23}$$

$\lambda/\ell = 1.0, \frac{1}{2}, \frac{1}{3}$ and $\frac{1}{4}$. Therefore, the minimum heave response will occur when the wave pumping is also a minimum, and likewise the maximum response occurs close to $\lambda/\ell = 2, \frac{2}{3}, \frac{2}{5}$, and $\frac{2}{7}$. The small differ-

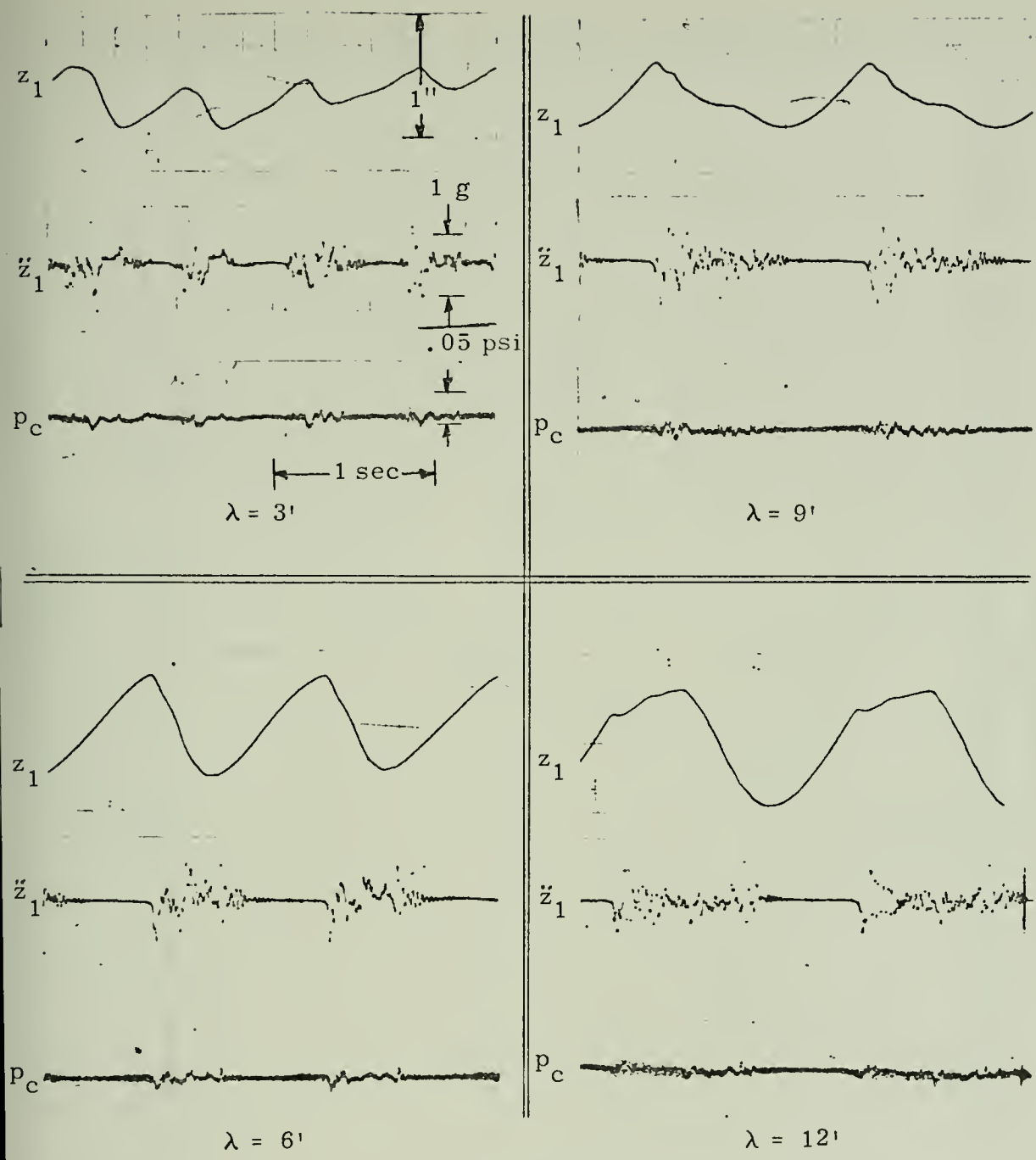

Abscissa

Time, 1 sec = 25 div.

Ordinate

z_1 Heave 1" = 20 div. p_c-p_a Press.

$\ddot{z}_1$ Accel, 1 g = 10 div. 1 psi = 100 div.

Fig. 4.3 Time Histories of Experimental Heave, Acceleration and Cushion Pressure.

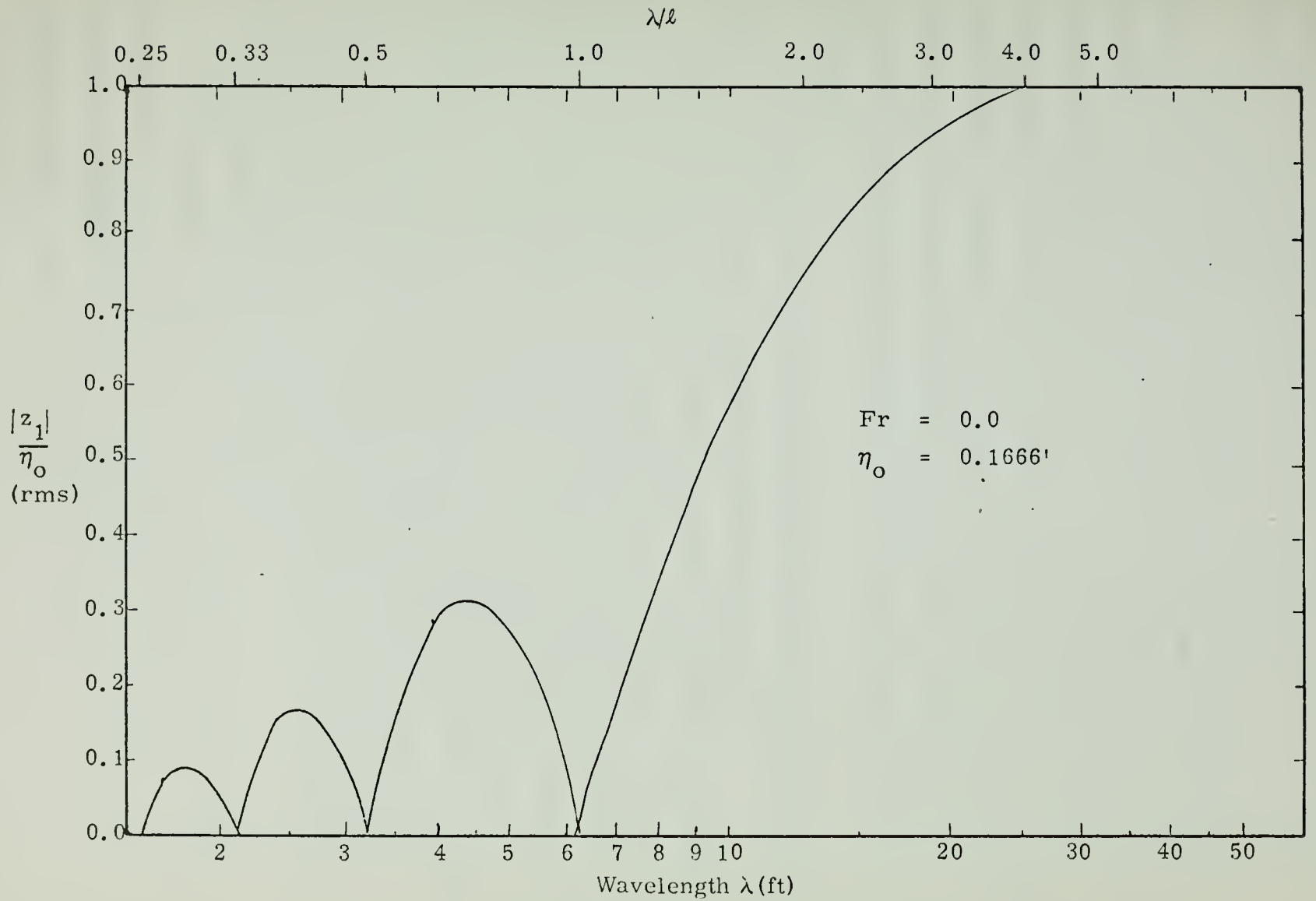

Fig. 4.4 Simulated Heave Motion Frequency Response.

ence between the simulation and the values in (23) is due to the effect of the natural heave frequency which is near $\lambda/\ell = 0.38$.

The large response characteristics at short wavelengths, which are due to the direct influence of wave pumping as well as to the resonance effect, result in relatively large heave acceleration (rms) values as indicated in simulation results, Fig. 4.5. This condition, which is generally known to occur in air cushion vehicles, is often referred to as "cobblestone" oscillation. It is evident when considering the operation of these craft over short wavelengths. This effect, though, was not verified from the experimental data, but is recommended for future verification.

The results of the heave motion and acceleration from simulations, Figs. 4.4 and 4.5, agree with the simulation studies in [1].

With the basic results of the heave motion presented, the simulations are now compared to the experimental test results. The heave motion frequency response data from several series of experimental tests are summarized in Fig. 4.6. Data for the response to waves of length λ = 1.5 - 12 ft, and height η_o = 2 in, indicate that the model exhibits the same general response as the experimental results. This is; the minimums and maximums along with the increasing heave response amplitude with wavelength are similar. Experimental data for wavelengths 3.1 - 4.6 were not available, Fig. 4.6; therefore, the results are not conclusive in this region.

The most interesting result, Fig. 4.6, is the shift in the experimental heave response minimums as compared to the model. The two primary minimums are at $\lambda/\ell = 0.35$ and 1.47. At the lower wavelengths another minimum appears near $\lambda/\ell = 0.22$.

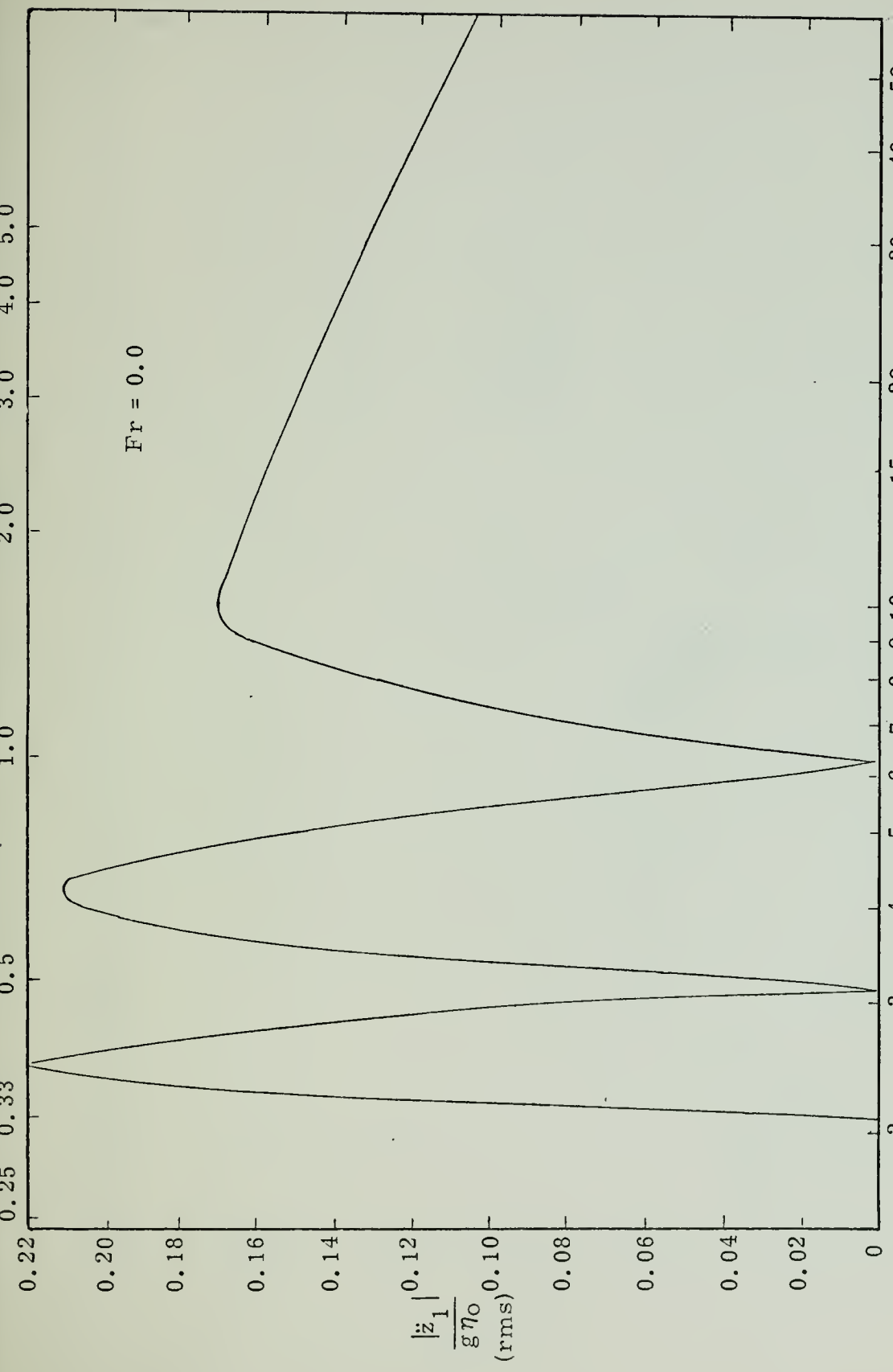

Fig. 4.5 Simulated Heave Acceleration Frequency Response.

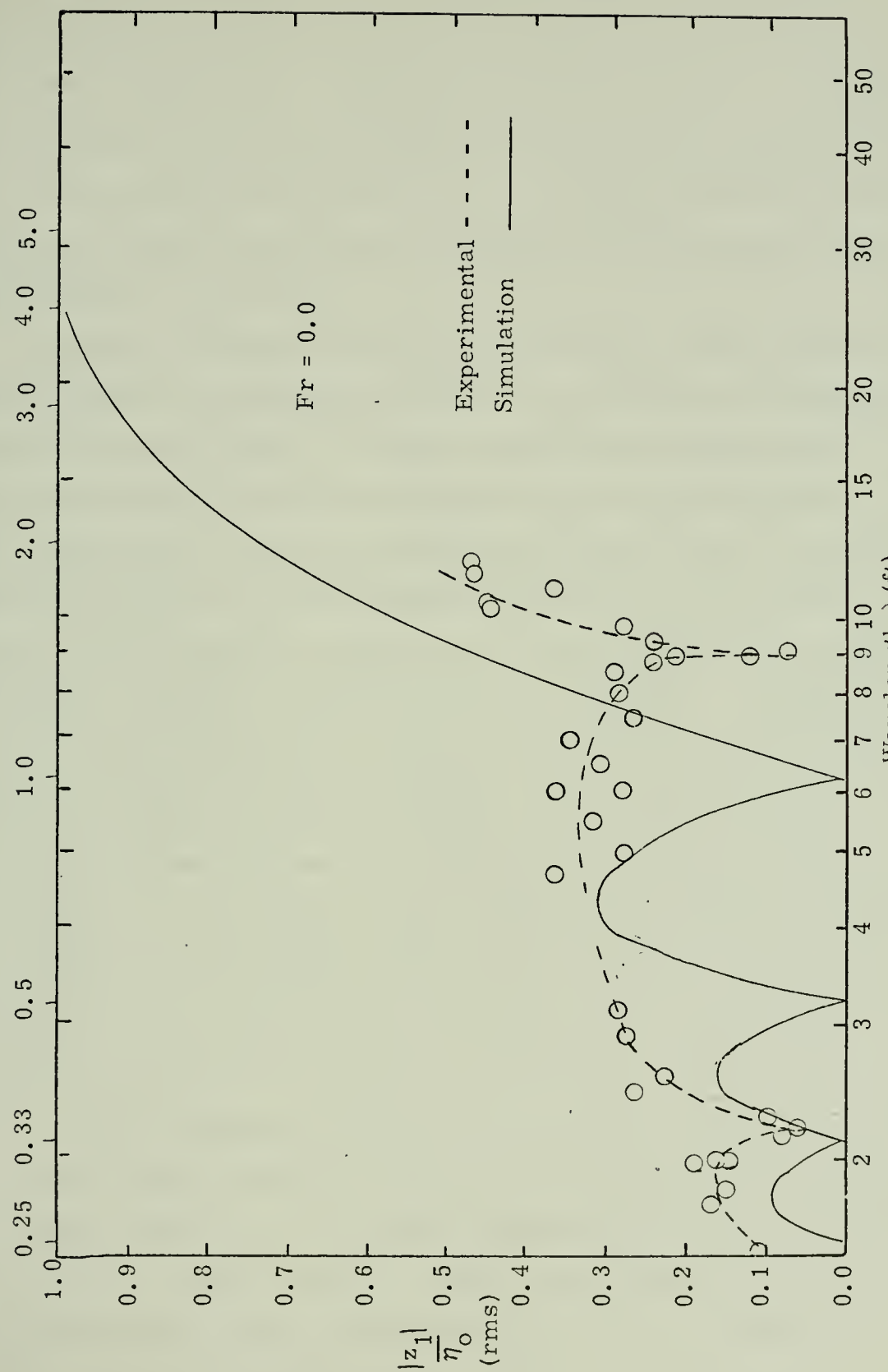

Fig. 4.6 Comparison of Experimental and Simulated Heave Motion Frequency Response.

In an effort to account for the differences between experimental and model results, several ideas were put forward based upon observations of the cushion waves. With the lack of data for λ = 3.1 - 4.6, the first assumption concerning the response in this area was to assume the heave response followed a smooth curve. This would then indicate that the primary minimum heave response shifts to the left and right of the model values λ = 0.5 and 1.0.

In order to determine what may cause this shift, observations of the wave profile photographically indicated some differences between the external and internal waves. Further experimental testing was performed by mounting wave probes internally and externally to the SES craft. Experimental results for various wavelengths, Fig. 4.7, indicate that the incoming wave is being altered in several ways. First the internal wave is lagging the external wave by 20-30 degrees at the lower wavelengths. Secondly, secondary waves are appearing. Thirdly, the internal wave is amplified at data values λ = 3.12', 6.5', and 9', and slightly attenuated at the other wavelengths. This indicates that the seals and, to a lesser degree, the sidewalls are creating an internal standing wave. For this reason, the minimum heave response would be expected to shift. The amount of shift would depend upon whether the standing wave or the external wave is dominant. The standing wave, having its own characteristic eigenvalue, could cause a shift in the system's natural frequency response away from the original model values.

There is some speculation that a dip in the heave response might occur in the region λ = 3.1 - 4.6 where experimental data were not available, Fig. 4.6. If this were true, then the results would indicate that the minimums have shifted to the right of model values. Again, the

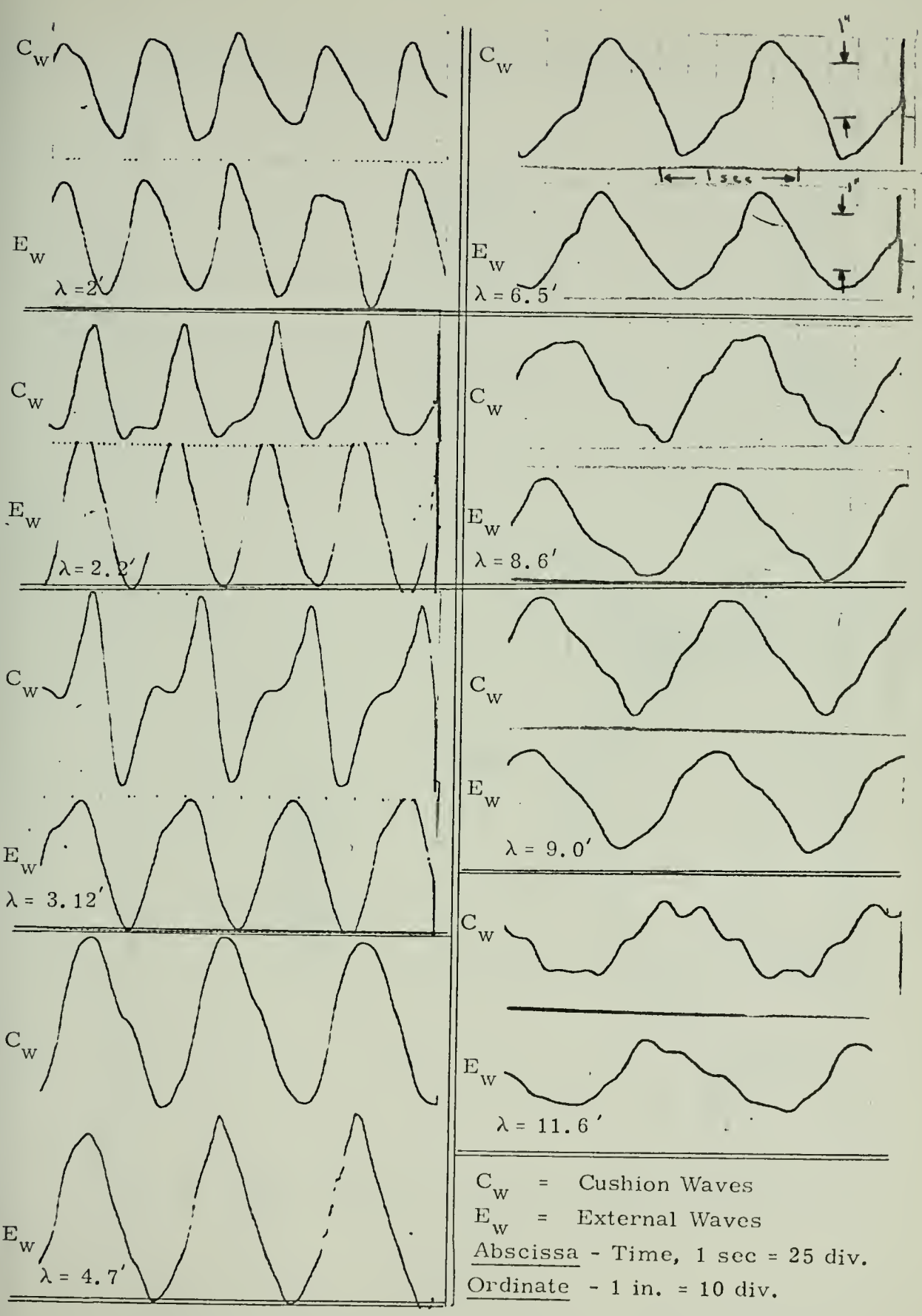

Fig. 4.7 Comparison of Cushion and External Waves.

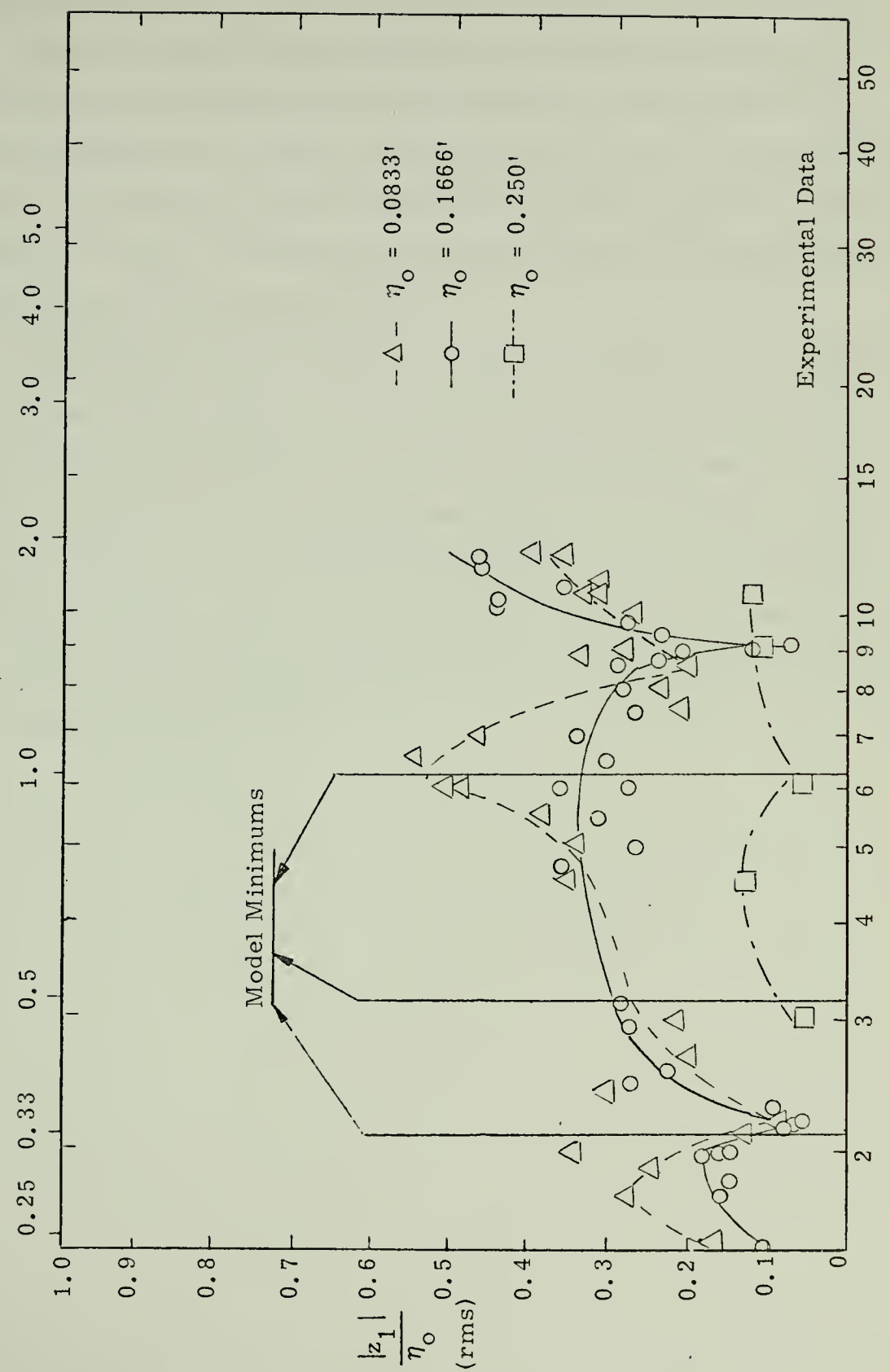

Fig. 4.8 Heave Motion Frequency Response for Various Wave Heights.

internal standing wave would be the main contributor to such a shift.

Since no further model simulations were performed that could account for the wavelength shift and experimental verification of the heave response at the missing wavelengths, this is left for future investigation. Additionally, investigation with the craft moving at a forward velocity is needed. Sufficient questions have arisen that will hopefully induce others to further the research.

Additionally, data comparisons of heave response to wave heights of 1, 2 and 3 inches, Fig. 4.8, indicate that heave damping increases with higher wave heights for $\lambda/\ell < 1.0$. The maximum and minimum heave response to waves of varying height appears to shift toward the model values as the wave height increases, Fig. 4.8. This might be expected in that the external wave dominates any internal standing wave.

This concludes the experimental tests conducted and the extent of verification of the simulation.

CHAPTER 5

SUMMARY AND RECOMMENDATIONS

5.1 Summary

Theoretical model simulations and experimental craft tests for the one degree of freedom heave motion of a surface effect ship have been conducted. The theoretical third order linearized model dynamical equations consider the following:

1. A constant air mass flow into the cushion.
2. Quadratic exit gap orifice restriction for air flow out of the cushion.
3. Conservation of momentum of the SES rigid body in the vertical mode.
4. Conservation of air mass inside the cushion.
5. Polytropic relationship between pressure, air mass and air volume.
6. Stationary model in x-y plane.
7. External force inputs and regular wave disturbances are the principal transients considered in analysis.

In order to simplify analysis and to verify the system's responses, linear analysis has been developed and the basic third order characteristic equation derived. A study of the linear model characteristics under external force inputs has been conducted for the SES ($\ell/b = 6.5$) with constant air flow. In the best fit of the transient response simulation of the model and the experimental data, the natural frequency and critical damping ratio of 9.2 rad/sec and 0.3, respectively, were determined. From theory based upon Stoker's formulation [5], the natural frequency and damping, based upon an oscillating free surface pressure field, were

also found to be in good agreement with the experimental results. The transient response characteristics of Model B (with air flow) did not appreciably alter the response of the craft when compared to Model A (without air flow). This was due to the time constant for filling the cushion being an order of magnitude greater than the system's natural heave frequency. The experimental results verified this. The value of damping was determined to be the critical measure in estimating the amplitude of the transient response. As would be expected, the increase in damping helps to decrease the effects of external disturbances.

The outcome, due to variations in seal design, was noted where the effective exit gap length under the seal influences the air loss. The solid seal design maximizes the effects of the nonlinear characteristics of the exit gap area, which, in turn, influences the heave motion, acceleration and cushion pressure. These results would likely be attenuated with flexible seals.

The sensitivity of vehicle performance to wavelength and wave height were studied with the following primary results:

1. Prediction of heave amplitudes from theory compared favorably with the experimental results. The relative amplitude to wave height ratio was found to decrease with increasing wave height for $\lambda/\ell \leq 1.5$ in the experimental tests. This is indicative that damping increases as the wave height increases.

2. The predictions of minimum wave pumping from theory, assuming the Froude-Krylov hypothesis, should occur near $\lambda/\ell = 1, \frac{1}{2}$, and $\frac{1}{3}$. Experimental evidence, though, indicates that at low speeds the primary wave is altered by the seals and sidewalls.

3. As a result of seal and sidewall effects upon the waves under the

cushion, the points of minimum and maximum heave motion are altered. Experimental evidence shows that the minimum wave pumping is shifted to the left and right of the two primary theoretical values. For this particular test craft, the minimums occurred at $\lambda/\ell = 0.38$ and 1.47. Comparisons of the inside and outside wavc profiles from experimental tests indicate a general lag in the wave under the craft whcn compared to the outside wave. Also the amplitude of the waves under the cushion is attenuated in some wavelengths while others are amplified at other wavelengths. These effccts are not considered in the simulation model and therefore account for the major difference between theory and experiment.

4. The sensitivity of acceleration levels to external disturbances was studied in the simulation model. The accelerations are 180 degrees out of phase to the heave motion. The acceleration (rms) response over a range of wavelengths in the simulation gives the "cobblestone" appearance with relative magnitudes increasing at shorter wavelengths. No experimental tests were conducted to verify this result.

Turning now to the experimental results, high frequency oscillations of the cushion pressure and accelerations were observed. This phenomenon occurred when the exit gap area was opening and closing. Thc air appcars to escape under the seals with bubbling action. This effect is not apparent in the simulation models since a smooth opening and closing of the exit area is considered. These high frequency oscillations, though, appear not to alter the basic craft hcave response. Also, there may bc somc water impact forces on the solid seals which could account for some of the high frequency accelerations.

In conclusion, the third order linear model equations are fair

representations of the model dynamics of the craft and air cushion. The principal differences in heave response between theory and experiment would appear to be attributable to the water dynamics under the cushion. The next step in the modeling must allow for this seal-water interaction and the resultant waves under the cushion.

5.2 Recommendations

1. A detailed study of the waves inside the cushion along with their cause, i.e., seals and sidewalls, and their effect upon the cushion dynamics is needed.

2. Modeling techniques as a result of 1 could, therefore, predict the system dynamics to a greater degree of accuracy.

3. Regions of applicability of the Froude-Krylov hypothesis should be established.

4. Although the quadratic orifice equations appear to predict fairly accurately the air mass flow from the cushion, measurements of the time lags induced by the air flow around the seals and their effects upon the overall dynamics should be considered in a more detailed study.

5. A study of the contribution to damping and added mass by the sidewalls would be a valid consideration not studied in this thesis. Slender body theory is suggested as one approach.

6. Further experimental model tests should be conducted with the craft moving with a forward velocity.

7. Acceleration amplitudes between theory and experiment need verification.

8. After completing the heave study, the pitch motion of the SES may be investigated.

APPENDIX A

EXPERIMENTAL FACILITIES AND TESTS

A.1 Introduction

The SES with length to beam ratio of 6.5 was selected for study in the experimental program of this thesis. Since little open and detailed literature is available on the motion (heave) characteristics of this particular SES, a test program was formulated and carried out. Results from the static, transient, and frequency responses were used in the simulation study.

A.2 Test Program

For the purpose of this thesis, the experimental test program was designed to accomplish measurements of (1) the static stiffness coefficient (displacement/load ratio) of SES, (2) the transient response to a step input in force, and (3) the frequency response of the SES to a series of regular waves.

A.3 Test Craft and Facility

Figure A.1 is a photograph of the SES craft in the tow tank with the tow carriage and associated instrumentation. The basic test craft dimensions and equilibrium testing conditions are given in Table A.1. The test craft's sidewall and deck were constructed from $\frac{1}{4}$-inch plexiglass. The sidewalls and seals at the bow and stern were shaped (faired) from styrofoam (Fig. A.2) and attached to the test craft. Note: the seals are inflexible and positioned for a particular equilibrium state. One advantage of building the test craft from plexiglass is the visual observation of the free surface inside the cushion. Photographs of the wave profile were taken from the side.

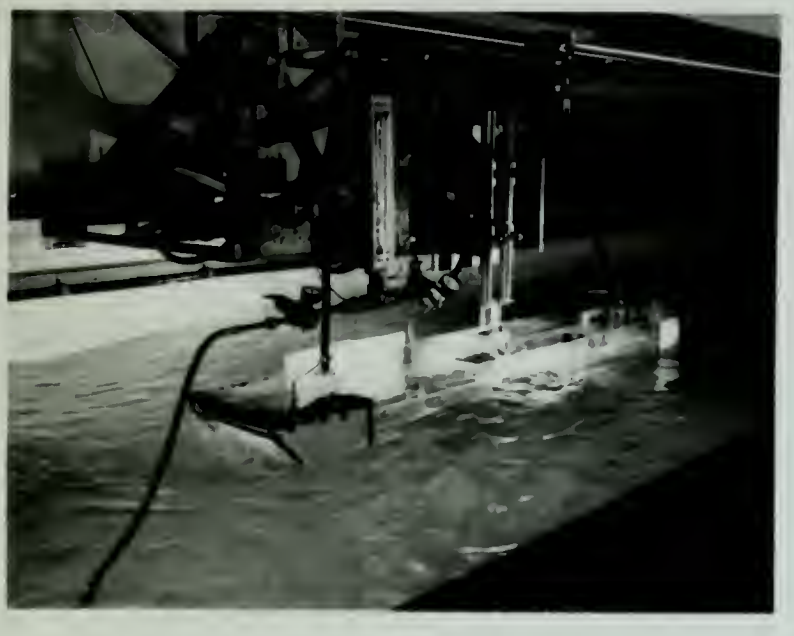

Fig. A.1 SES Tow Tank Model Attached to Carriage.

Fig. A.2 SES Bow and Seal Configuration.

TABLE A.1

SES MODEL CHARACTERISTICS

Cushion Length, ℓ(ft)	6.26
Cushion Beam, b(ft)	0.96
Length Beam Ratio	6.5
Length Overall, L(ft)	6.66
Beam Overall, B(ft)	1.19
Cushion Area, A_b(ft^2)	6.00
Sidewall Height, z_t(ft)	0.328
Cushion Height, z_c(ft)	0.25
Sidewall Thickness, y_{sw}(ft)	0.115
Vertical Center of Gravity, (ft)	0.386
Longitudinal Center of Gravity, (ft)	3.27 from stern
Model Weight, (lb)	37.5
Specific Weight Density, (lb/ft^3)	1.0
Air Supply Flow Rate #1	29 $ft.^3$/min (STP)
#2	19 $ft.^3$/min (STP)
Air Density	0.075 lb/ft^3
Water Density	62.4 lb/ft^3

Pressurization of the cushion was accomplished by two pressurized supply lines, which were 3/8-inch in diameter, located near the bow and stern. Figure A. 3 illustrates the air supply and instrumentation involved. The air flow, hovering height, and craft weight may be adjusted independently. Nonequilibrium conditions were simulated by introducing regular waves. Several pressure transducers, wave probes, a heave rod, an accelerometer and an external flow meter were provided to accomplish quantitative studies. A chart recorder was available for recording each response.

A. 4 Static Response

The static response for craft height versus load was conducted by varying the craft weight and measuring the vertical displacement from the heave rod. See Fig. A. 4 for results. The observed stiffness was approximately linear over the operating range. The linearized spring coefficient $(\hat{k}_1 + \hat{k}_2)$ is equal to 435 ± 10 lb/ft.

A. 5 Dynamic Response

Transient responses were performed by removing weight from the craft and allowing it to reach a new equilibrium. This is equivalent to a step input in force. Transient performance data for heave, acceleration, and pressure were obtained.

The frequency response tests were performed by passing waves of various lengths and heights past the stationary SES. Response data were recorded for heave, acceleration, pressure, and the wave profile inside and outside of the cushion. Due to the noticeable difference between the free surface inside and outside the cushion, two different means of measuring this response were devised. Initially, photographs were

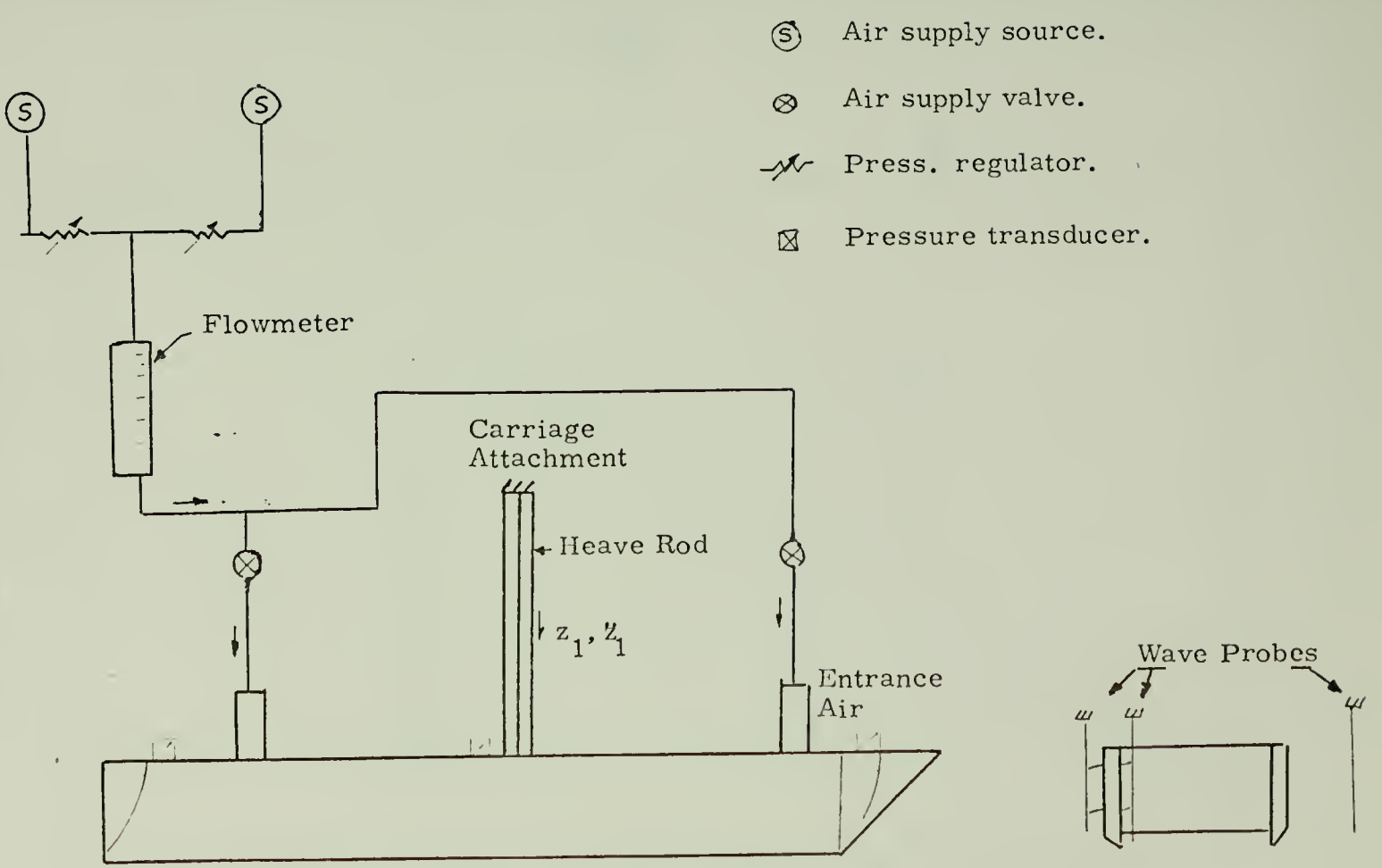

Fig. A.3 Experimental Test Apparatus.

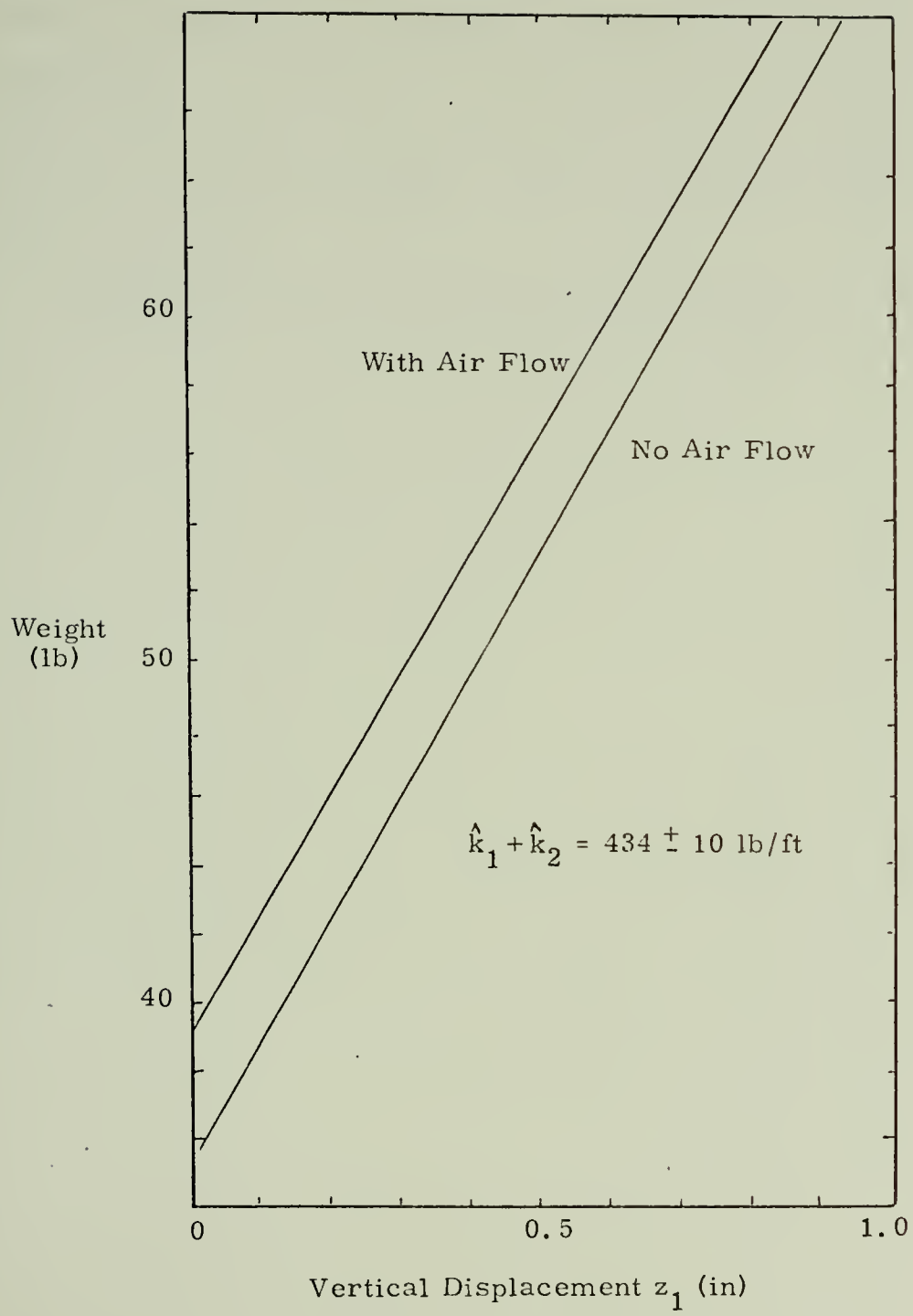

Fig. A.4 Experimental Stiffness Coefficient of SES.

taken of the inside and outside waves through a viewing window from the side of the tow tank. From these photos it is possible to observe the variance in the waves, but quantitative data analysis requires better photography. The second means of obtaining the time history of the cushion wave profile was by attaching wave probes at midship to the sidewall, both inside and outside. The wave profile, relative to the craft, was obtained.

Discussion of the results of these tests is found in the main text.

APPENDIX B

ADDED MASS AND DAMPING FOR OSCILLATING FREE SURFACE

Figures B.1 and B.2 were used to estimate the cushion added mass and damping.

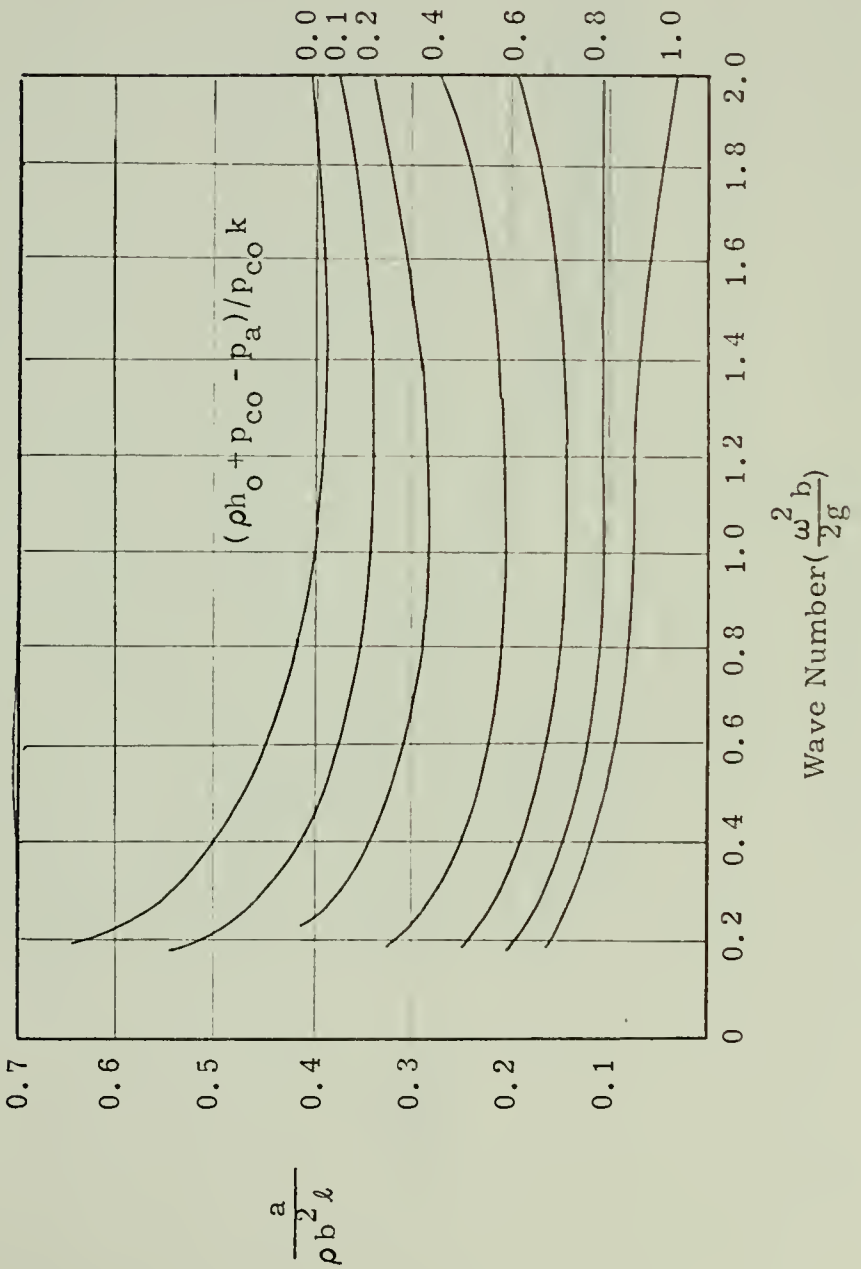

Fig. B.1 Added Mass Coefficient from [5].

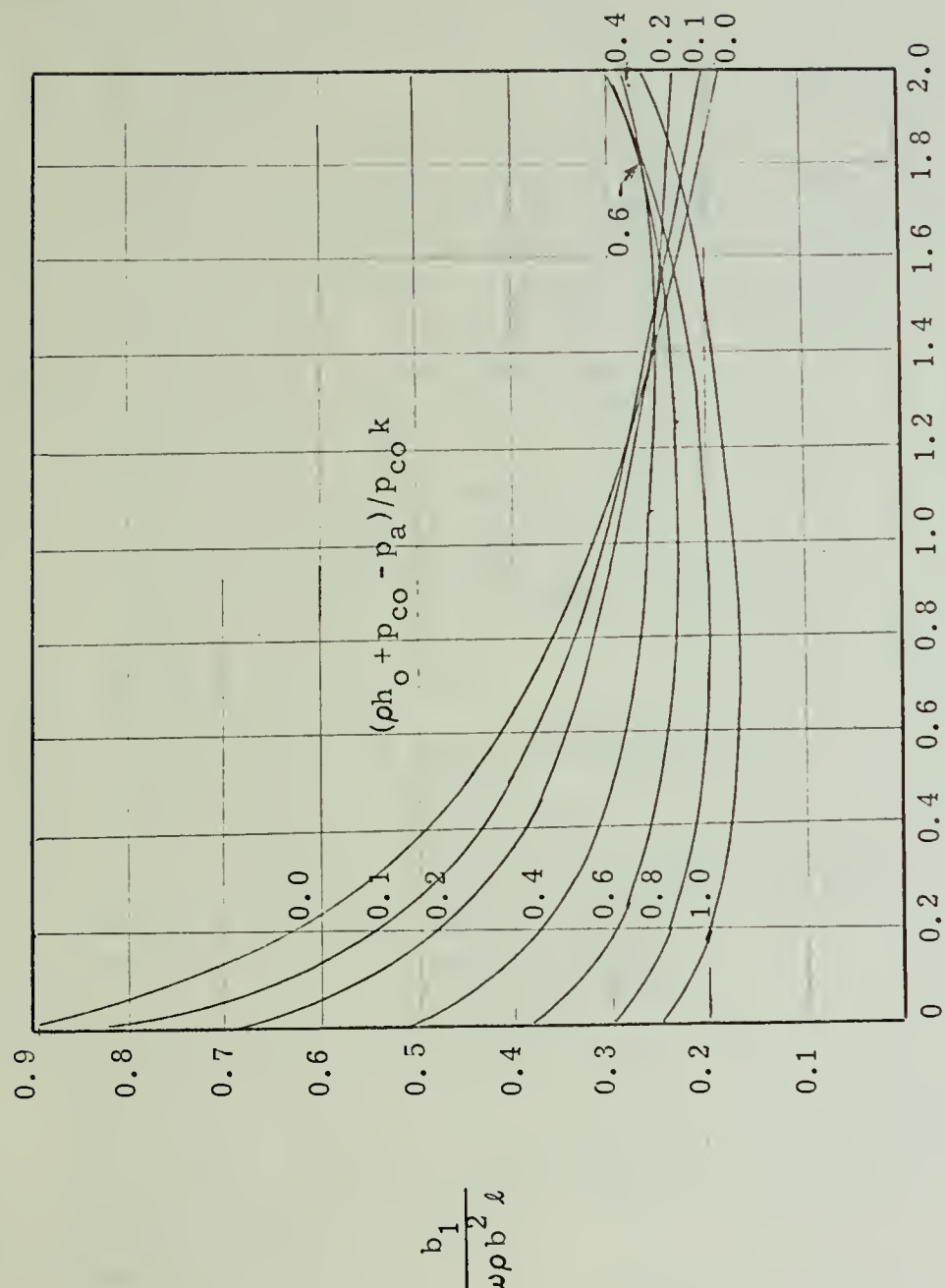

Fig. B.2 Damping Coefficient from [5].

```
C      HEAVE DYNAMICS OF SURFACE EFFECT SHIP
C      DIGITAL SIMULATION USING DYSYS (SUBROUTINE)

C            VARIABLES LISTED AS FOLLOWS
C    A= ADDED MASS LB SEC2/FT
C   AB= CUSHION AREA (FT**2)
C   AE=EQUIL. AIR EXIT AREA FROM SEALS (FT**2)
C  AEB= EXIT AREA AT BOW (FT**2)
C  AES= EXIT AREA AT STERN (FT**2)
C    B= DAMPING  (LB*SEC/FT)
C   CO, CE = ENTRANCE AND EXIT RESISTANCE COEF.  (0.6)
C   FR= AIR TEMP (F)
C    G= GRAVITY 32.2 FT/SEC**2
C   H2= EQUILIBRIUM HEIGHT OF CUSHION (FT)
C   H1= CONSTANT FOR EQUILIBRIUM OF EXIT AIR GAP UNDER SEAL (FT)
C   PA= AMBIENT AIR PRESSURE ABS (LB/FT2)
C   PC=  CUSHION PRESSURE ABS(LB/FT2)
C   PK= POLYTROPIC CONSTANT  (1.2)
C   QA= MASS AIR FLOW RATE INTO CUSHION (SLUG/SEC)
C   RW= WATER DENSITY (LB*SEC**2/FT**4)
C  RWS= AIR DENSITY (LB*SEC**2/FT**4)
C   TN= WAVE HEIGHT (FT)
C    U= FORWARD SPEED (FT/SEC)
C    W= CRAFT WEIGHT (LB)
C   WF= FREQ OF WAVES (RAD/SEC)
C   WL= WAVE LENGTH (FT)
C   WM= CRAFT MASS,LB-SEC2/FT)
C   WW= ENCOUNTER FREQ FOR HEAD SEAS (RAD/SEC)
C   XB= CUSHION LENGTH (FT)
C   YB= CUSHION WIDTH (FT)
C  YSW= SIDEWALL WIDTH (FT)
C   ZB= SEAL HEIGHT (FT)
C  ZIN= AVE. WAVE HEIGHT UNDER CUSHION (FT)
C  ZOB= WAVE HEIGHT AT BOW (FT)
C  ZOS= WAVE HEIGHT AT STERN (FT)
C   Y(1)=Z1=POSITION OF CRAFT
C   Y(2)=F(1)= VERTICAL VELOCITY OF CRAFT (FT/SEC)
C   Y(3)= AIR MASS IN CUSHION  (SLUG)
C   Y(5)=PC=CUSHION PRESSURE (LB/FT2)
C   F(2)= ACCELERATION OF CRAFT (FT/SEC**2)
C   F(3)= AIR MASS FLOW RATE (SLUG/SEC)
C   Y(9)= INPUT WAVE HEIGHT (FT)
C   Y(14)= GAP HEIGHT FOR BOW AND STERN (AVE) (FT)
      SUBROUTINE EQSIM
      COMMON T,DT,Y(20),F(20),STIME,FTIME,NEWDT,IFLRT,N
      IF (NEWDT) 1,3,2
1     READ(8,10) XB,YB,YSW,ZSW,W,FR,QA,H1,H2,A,B,TN,WL,U,PO,AE,PMC
10    FORMAT(8F10.3)
14    FORMAT(1F10.2)
      RW=62.4
      TN=TN/(12.0*2.0)
      WM=W/32.2
      G=32.2
      AB=XB*YB
```

```
      PA=2116.8
      TK=53.34*(460.0+FR)
      RWS=PA/TK
      WMA=WM+A
      WF=(2.0*3.142*G/WL)**0.5
      WW=WF+(WF**2.0)*U/G
      CO=0.6
      CE=0.6
      PHASE=3.142*XB/WL
      R=TN*YB*WL*SIN(PHASE)/(3.142*AB)
      F(2)=0.00002*5
      F1=0.00021/WMA
      F1=0.2
      PK=1.2
      PT=HO*RW/(PK*PO)+1.0
      PK3=CO*(2.0*RW*S/G)**0.5*AE*0.5/(PO-PA)**0.5
      PK4=CO*(2.0*RW*S/G)**0.5*2.0*YB*(PO-PA)**0.5
      C11=RW/PT
      C13=H2*RW/PMC
      D12=-RW/PT
      A21=-(RW*XB*YSW*2.0+AB*C11)/WMA
      A22=-5/WMA
      A23=-AB*C13/WMA
      B21=1.0/WMA
      B22=(RW*XB*YSW*2.0-AB*D12)/WMA
      A31=-PK3*C11-PK4*(-1.0+C11/RW)
      A33=-PK3*C13-PK4*C13/RW
      B32=-PK3*D12-PK4*(1.0+D12/RW)
2     WWT=WW*T
      ZOB=TN*SIN(WWT+PHASE)
      ZOS=TN*SIN(WWT-PHASE)
      ZIN=R*SIN(WWT)
      Y(5)=C11*Y(1)+C13*Y(3)+D12*ZIN
      Y(9)=-TN*SIN(WWT)/0.1
      Y(10)=-Y(1)/0.10
      Y(11)=-Y(2)/0.50
      Y(12)=-F(2)/10.0
      Y(13)=Y(3)/0.5
      Y(14)=AE/(2.0*YB)*10.0
      Y(15)=Y(5)/10.0
      AEB=YB*(H1+(PO  -PA)/RW+ZOB-Y(1))
      AES=YB*(H1+(PO  -PA)/RW+ZOS-Y(1))
      IF(AEB.LE.0.0) AEB=0.0
      IF(AES.LE.0.0) AES=0.0
      AE=AEB+AES
      PK3=CO*(2.0*RW*S/G)**0.5*AE*0.5/(PO-PA)**0.5
      A31=-PK3*C11-PK4*(-1.0+C11/RW)
      A33=-PK3*C13-PK4*C13/RW
      B32=-PK3*D12-PK4*(1.0+D12/RW)
3     F(1)=Y(2)
      F(2)=A21*Y(1)+A22*Y(2)+A23*Y(3)+B21*F1+B22*ZIN
      F(3)=A31*Y(1)+A33*Y(3)+B32*ZIN
```

REFERENCES

[1] Kaplan, Paul, and Sydney Davis, "A Simplified Representation of the Vertical Plane Dynamics of SES Craft", AIAA Paper No. 73-314, AIAA/SNAME Advanced Marine Vehicles Conference, February 25, 1974.

[2] Wormley, D. N., D. P. Garg and H. H. Richardson, "A Comparative Study of the Nonlinear and Linear Performance of Vehicle Air Cushion Suspension Using Bond Graph Models", Transactions of the ASME Journal of Dynamic System, Measurement, and Control, September 1972.

[3] Wormley, D. N., D. P. Garg and A. B. Boghani, "Nonlinear and Finite Pad Length Performance of Vehicle Air Cushion Suspensions". Prepared for Department of Transportation, Washington D. C., EPL-72-7266-1, February 1972.

[4] Karnopp, D., and R. C. Rosenberg, "Analysis and Simulation of Multiport Systems", The MIT Press, Cambridge, Massachusetts, 1968.

[5] Ogilvie, T. Francis, "Oscillating Pressure Fields on a Free Surface", University of Michigan College of Engineering, No. 030, September 1969.


Thesis
D475
Dewey
153597
Heave dynamics of a
surface effect ship.
30 SEP 74
DISPLAY
Thesis
D475
Dewey
153597
Heave dynamics of a
surface effect ship.